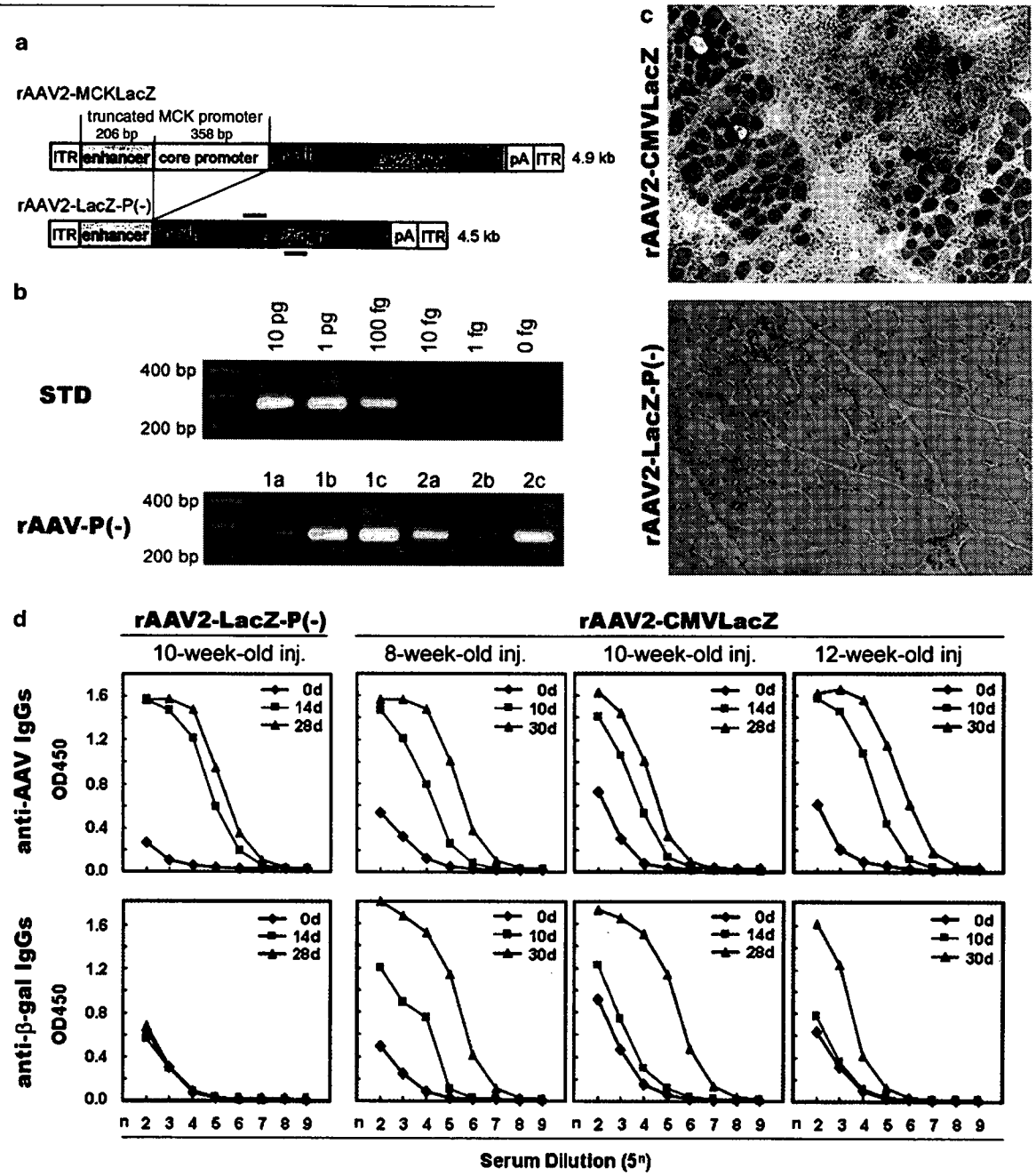

Figure 4 Injection of the promoter-deleted rAAV2 showed negligible cellular infiltration in canine muscle. The promoter-deleted rAAV2, rAAV2-LacZ-P(−) (5×10^{12} vg/500 μl/site) was injected into skeletal muscles of 10-week-old beagle (dog 902), and the injected muscles and sera were analyzed at 2 and 4 weeks post-injection. (**a**) Schematic illustration of rAAV2-LacZ-P(−). Upper and lower bars correspond to primer positions used for detection of genome in Figure 4b. (**b**) Detection of rAAV genome DNA in the rAAV-LacZ-P(−)-injected canine muscles. Total DNA was extracted from the muscle sections, and *LacZ* DNA fragment (275 bp) was amplified from 200 ng of template DNA by PCR. Results at 2 weeks after the injection were shown. The numbers 1a–2c show individual identities of the muscle specimen divided into pieces. Vector genomes were detected in all samples, but amplified levels were different between muscle blocks. STD: quantity standard of AAV vector plasmid; rAAV-P(−): rAAV2-LacZ-P(−) genome. (**c**) Cellular infiltrations were rarely observed in the rAAV2-LacZ-P(−)-injected canine TA muscle (sample 1c). Canine muscles were injected with the rAAVs expressing β-gal or no transgene, and the muscle blocks were sectioned and stained with H&E staining at 2 weeks after the injection. All muscle samples from rAAV2-CMVLacZ (1a–2c) showed minimal cellular infiltration. Magnification: × 200. (**d**) Detection of antibodies against AAV particles and β-gal in the rAAV-treated dogs. Sera from dogs injected with rAAV2-LacZ-P(−) (dog 902) or rAAV2-CMVLacZ (dogs 0338, 901 and FF04, also see Table 1) were analyzed by using the ELISA technique for the presence of IgG antibodies against AAV particles and β-gal protein at 0, 2 and 4 weeks after the injection. AAV, adeno-associated virus; β-gal, β-galactosidase; ELISA, enzyme-linked immunosorbent assay; rAAV, recombinant AAV.

Next, we measured the anti-AAV IgG type antibodies in the serum of the treated dogs (Figure 4d). In the rAAV2-LacZ-P(−)-injected dog at 2 and 4 weeks after the injection, anti-AAV2 antibodies were detected at high levels similar to those in rAAV2-CMVLacZ-injected dogs, but antibodies against β-gal were undetectable. This indicates that antibodies against AAV particles were developed in rAAV2-LacZ-P(−)-injected dogs but did not lead to elimination of transduced cells.

Immunosuppression of the rAAV-injected dogs slightly improved the expression of the transgene

To test whether immunosuppression could improve transduction by rAAV-2 in canine muscle, we daily administered cyclosporine to the rAAV2-CMVLacZ-injected dogs from −5 day of the injection until the sampling day of muscle specimens (Table 2A). Unexpectedly, β-gal expression in the injected muscles of cyclosporine-treated dogs was as low as that in the untreated dogs. Only the extensor digitorum longus (EDL) muscle of dog 403 expressed β-gal at a high level at 2 weeks after the injection, although a large number of infiltrating cells with CD4+ or CD8+ cells and upregulation of MHC class I and -II were detected (data not shown). In contrast, in the rAAV2-CMVLacZ-injected extensor carpi ulnaris (ECU) muscle of dog 403 at 2 weeks post-injection, β-gal expression was much lower than that in the EDL muscle. Thus, as a whole, cyclosporine alone could not effectively improve transduction of rAAV2-CMVLacZ.

Mycophenolate mofetil (MMF) suppresses the functions of T lymphocytes in a different way with cyclosporine. Therefore, to suppress immune responses more effectively, we treated the rAAV2-CMVLacZ-injected dogs both with MMF and cyclosporine. MMF was daily administrated from 0 day to the day of sampling (Figure 5 and Table 2B). This combined immunosuppression significantly increased the numbers of β-gal-expressing fibers, compared with those in the untreated muscles when examined at 2 weeks after the injection, but cellular infiltration was still observed. Some CD4+ or CD8+ cells and upregulation of MHC class I and -II in infiltrating cells and myofibers were detected in rAAV2-CMVLacZ-injected muscle (data not shown). After 4 weeks, β-gal expression significantly decreased together with increasing infiltrating cells. These results indicated that combination of cyclosporine and MMF could partially improve the transduction efficiency of a rAAV2 in canine muscles.

Immunological background of enhanced immune responses in dogs

We next investigated possible differences in immune responses between mice and dogs, which might explain why rAAV2 injection evoked strong immune responses in canine muscles. To this end, we prepared single-cell suspension from spleens of untreated dogs or mice, stimulated them with AAV capsids and purified β-gal protein *in vitro*, and assayed the secretion of interferon-γ (IFN-γ) by enzyme-linked immunosorbent assay (ELISA; Table 3). We also stimulated the splenocytes with two major mitogens for T lymphocytes, concanavalin A (ConA) and phytohemagglutinin (PHA). When stimulated with ConA or PHA, canine splenocytes secreted much larger amount of IFN-γ into the culture medium than murine cells. Furthermore, canine cells secreted slightly higher levels of IFN-γ in response to β-gal or rAAV2 capsid proteins than murine cells. These results suggest that canine splenocytes are innately more susceptive to

Table 2 Gene transfer of rAAV2-CMV-LacZ into canine skeletal muscles under immunosuppression

Animal[a]			*Injection*[b]	*Cyclosporine*	*Expression*[c]		*Infiltration*[d]	
(A) Cyclosporine alone								
Injection at 5 weeks				Dose/kg/day	2 weeks	4 weeks	2 weeks	4 weeks
601	B	M	(6.0×10^{12} vg/500 μl)	20 mg	−		+	
Injection at 8 weeks								
1103	B	M	(5.0×10^{10} vg/500 μl)	25 mg	−, −	±, −	±, ±	+, −
1102	B	M	(6.0×10^{11} vg/500 μl)	25 mg	±, −	±, −	+, ±	+, +
Injection at 11 weeks								
403	B	M	(7.7×10^{12} vg/500 μl)	20 mg	+++, +[e]	+, ±	+, +	+, +
703	B	M	(5.0×10^{12} vg/500 μl)	50 mg	−		±	
Animal[a]			*Injection*[b]	*Cyclosporine, MMF*	*Expression*[c]		*Infiltration*[d]	
(B) Cyclosporine and MMF								
Injection at 10 weeks				Dose/kg/day	2 weeks	4 weeks	2 weeks	4 weeks
VC1XE	B	M	(5.0×10^{11} vg/500 μl)	25 mg, 30 mg	++, +	±, +	+, ±	+, ++
TC2XE	B	M	(5.0×10^{12} vg/500 μl)	25 mg, 30 mg	±, +	+, −	+, +	++, +
Injection at 12 weeks								
1902	B	M	(5.0×10^{11} vg/500 μl)	25 mg, 30 mg	+	++	±	±

Abreviations: B, beagle; ECU, extensor carpi ulnaris; EDL, extensor digitorum longus; F, female; M, male; MMF, mycophenolate mofetil.
[a–d]See Table 1.
[e]+++ was seen in an EDL muscle, whereas + was in an ECU muscle.
In [c] and [d], individual results of the injected muscles were shown.

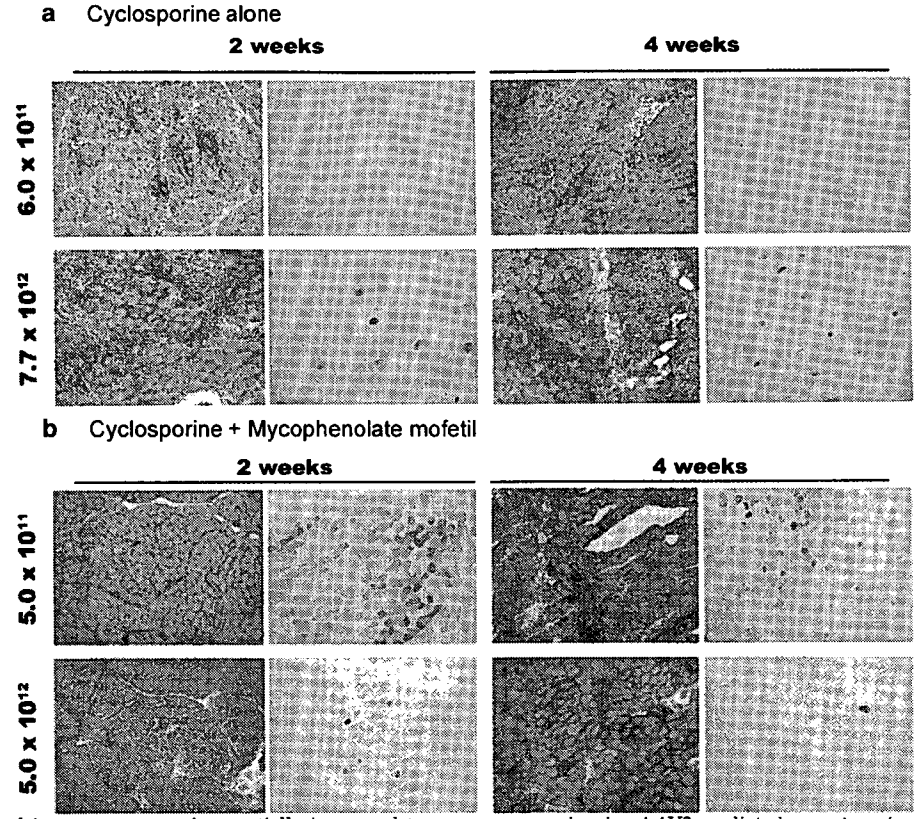

Figure 5 Combined immunosuppression partially improved transgene expression in rAAV2-mediated gene transfer into canine muscle. Representative H&E and X-gal stainings showing improvement in the transduction efficiencies of rAAV2-CMVLacZ at 2 and 4 weeks after the injection under immunosuppression (also see Table 2). The rAAV (5.0×10^{11}–7.7×10^{12} vg/site) was injected into TA and ECU muscles of beagles, and the dogs were daily treated with cyclosporine alone (**a**) or combination of cyclosporine and MMF (**b**). The muscle of dog 1102 was injected with rAAV at a dose of 6.0×10^{11} vg (upper panels in **a**). Dog 403 was injected with rAAV at a titer of 7.7×10^{12} vg; beagle VC1XE was injected with rAAV at a dose of 5.0×10^{11} vg (upper panels in **b**). TC2XE was injected with 5.0×10^{12} vg rAAV (lower panels in **b**). Magnification: × 100. ECU, extensor carpi ulnaris; H&E, hematoxylin and eosin; MMF, mycophenolate mofetil; rAAV, recombinant adeno-associated virus; TA, tibialis anterior; X-gal, 5-bromo-4-chloro-3-indolyl-β-D-galactopyranoside.

immunogens or mitogens than murine ones, and this immunological difference might underlie severer immune responses to rAAV2 injection in dogs than in mice.

Discussion

rAAV2 drives a long-term expression of microdystrophin genes in skeletal muscles of dystrophic mice,[9] therefore it is an attractive tool for treatment of DMD. To test the efficacy and safety of rAAV-mediated gene transfer into skeletal muscle of larger animal models, we directly injected rAAV2 encoding β-gal into skeletal muscle of normal dogs and examined the β-gal expression at several time points. Unexpectedly, we found that rAAV2-mediated gene transfer elicits strong immune responses against the transgene product in canine skeletal muscles. The mechanisms of enhanced immune reactions after rAAV2 injection seen in normal dogs need to be clarified before applying rAAV-mediated gene therapy to boys with DMD.

rAAV2 efficiently transduces canine muscle in vitro *but not* in vivo

In mice, β-gal expression is maintained for a long time after rAAV-CMVLacZ injection into muscle.[8] In contrast, low levels of β-gal expression and numerous infiltrating cells were observed in the rAAV2-CMVLacZ-injected canine muscle. Surprisingly, rAAV2 infected and transduced canine myotubes more effectively than murine myotubes *in vitro* (Figure 1). Therefore, we conclude that the low expression of the transgene in dog muscle is not due to the lack of receptors for the AAV2 on canine muscle fibers.

Cytotoxic immune response against the transgene product

Immunosuppression reduced cellular infiltration in rAAV2-CMVLacZ-injected muscle and partially rescued the β-gal expression in myofibers, suggesting that cytotoxic T-cell responses to transduced muscle fibers are largely responsible for the elimination of β-gal-positive myofibers in the injected muscle. Furthermore, intramuscular injection of the promoter-deleted rAAV2, which can infect the muscle (Figure 4) but express no β-gal (data not shown), induced much less cellular infiltration in canine muscle than the rAAV2-CMVLacZ. This observation suggests that massive destruction of the transduced muscle cells is mainly due to cellular immunity against the transgene product but not against AAV capsid proteins.

Table 3 IFN-γ release assay in murine and canine splenocytes

Immunogen		*IFN-γ (pg/ml)*	
		Mouse	*Dog*
None	—	<9.4	<32
β-gal	500 ng	<9.4	<32
	5 μg	<9.4	166±5
	50 μg	334±20	1316±122*
rAAV	1×10^8 vg	<9.4	<32
	1×10^9 vg	<9.4	<32
	1×10^{10} vg	<9.4	59±19
ConA	5 ng	<9.4	<32
	50 ng	<9.4	4928±162
	500 ng	6750±132	57 567±6374*
	5 μg	4095±474	65 050±5467*
PHA	50 ng	<9.4	49±7
	500 ng	<9.4	5227±479
	5 μg	2683±253	43 833±4488*
	50 μg	5453±349	60 133±6616*

Abbreviations: β-gal, β-galactosidase; ConA, concanavalin A; ELISA, enzyme-linked immunosorbent assay; IFN-γ, interferon-γ; PHA, phytohemagglutinin; rAAV, recombinant adeno-associated virus.
Splenocytes were stimulated with various doses of immunogens, such as β-gal, rAAV particle (rAAV), ConA and PHA, and secreted level of murine and canine IFN-γ in culture medium were measured by ELISA. Data are expressed as means±s.d., and significant differences (*$P<0.01$) between mouse and dog were shown.

There have been several papers reporting studies of rAAV-based gene transfer into canine skeletal muscle. Most of them were gene transfer studies for hemophilia B dogs, and reported that cellular immune responses against Factor IX, were nearly absent in dog models of hemophilia B.[15–19] The difference between studies of hemophilia and ours might be explained by the antigenicity of the transgene products. When we injected rAAV2-CMVM3 expressing M3 microdystrophin[7] into skeletal muscles of normal dogs, cellular infiltration was considerably reduced (data not shown), indicating that lowering the immunogenicity of therapeutic genes is important to improve the efficiency of gene therapy. In addition, nonsecreted, intracellular proteins might tend to evoke cellular immunity, compared with secreted proteins, like Factor IX.

We showed quite low expression of β-gal in rAAV2-CMVLacZ-injected muscle, whereas AAV genome and *LacZ* mRNA in rAAV-CMVLacZ-injected muscle were detected even at 8 weeks after the injection (Figure 2). The gap between *LacZ* mRNA level and β-gal protein cannot be fully explained at present. This might be simply due to time lag between transcription and translation of the transgene, or translation of β-gal might be repressed in inflammatory muscles.

Immunity against AAV2 capsid in dogs and humans

Promoter-deleted rAAV2 injection did develop antibodies against the AAV2 capsid after the injection into the skeletal muscle (Figure 4d), but did not evoke strong immune reactions in muscle, suggesting that cytotoxic T cells targeting the AAV2 capsid protein were not or minimally activated. This observation is consistent with the previous reports that cellular immune response to the AAV capsid was absent in hemophilia B dogs.[17–19] However, it is still unclear whether cellular immune response against the AAV2 capsid proteins is completely absent in dogs. Because even a low-level response could be problematic in the clinic, immunity to the AAV2 capsid proteins should be carefully monitored in dog models. In contrast, it has been recently reported that liver-directed rAAV2 transfer for human trial of hemophilia B led to destruction of transduced hepatocytes by cell-mediated immunity targeting the AAV2 capsid.[13] The authors suggest that T-cell immunity against the AAV2 particles might be associated with peptide sequence within the AAV2 capsid which had a high predicted binding potential to *B*0702* molecule of human MHC class I. This may explain why cell-mediated immune response against the AAV2 capsid protein was activated in humans.

Backgrounds of immune responses in dogs and mice

We measured the levels of IFN-γ secreted from canine or murine splenocytes after stimulation with β-gal, rAAV2 viral particles, ConA or PHA *in vitro*. Although biological activities (e.g., EC_{50}) of canine IFN-γ might be different from those of murine IFN-γ, it is likely that canine immune system is more sensitive to foreign antigens, such as β-gal. We also showed that canine splenocytes secrete much larger quantity of INF-γ than murine splenocytes when exposed to ConA or PHA. The higher levels of overall immune activation in dogs than in mice might be responsible for rapid development of immune response to rAAV2-mediated gene transfer into canine skeletal muscle, and might be partly explained by the different sanitary status of murine and canine colonies.

Antigen-presenting cells (APCs) in skeletal muscle play an important role in development of immunity to transgene products.[8,20] Therefore, it is also possible that rAAV transduces APCs more efficiently in dogs than in mice.

Threshold hypothesis for detrimental immune reaction

A previous study showed that systemic delivery of rAAVs, such as isolated limb perfusion (ILP) elicited less immune response than local injection.[19] Other study in hemophilia B dogs suggested that local Factor IX antigen dose in rAAV-injected muscles would be a critical parameter for risk of developing neutralizing antibody in dog.[18] The authors discussed that vector dose of 2×10^{12} vg/site and 8.5×10^{12} vg/kg might represent a threshold at which an inhibitory anti-Factor IX was or was not induced. These observations might indicate that the local concentration of the rAAV particles and its gene product is an important factor for establishment of immunity against rAAVs. Direct injection of rAAV2-CMVLacZ particles into muscle might cause the excessive expression of β-gal within a small area, and thereby mount strong cellular immune responses against gene products. Recently, we observed that pseudo-typed rAAV2/8 efficiently delivered the transgene into canine muscle (Ohshima *et al.*, unpublished observation). The expression of β-gal from rAAV8-CMVLacZ distributed more widely, and more evenly within the muscle than rAAV2-CMVLacZ after direct injection into canine

muscle. We hypothesize that widespread transduction of myofibers at a low dose of a rAAV2/8 could escape the establishment of immunity against the transgene products. New serotypes of AAVs, such as AAV8 or AAV9 can deliver the transgene into musculature of the whole body via circulation.[21,22] These vectors might overcome the immunological problems that we encountered in rAAV2-mdiated gene transfer into canine muscles.

In conclusion, we found that intramuscular administration of rAAV2-CMVLacZ elicited rapid and severe immune responses against the transgene product in wild-type dogs. This has not been observed in mice. It is important to understand well the mechanisms of immune reactions observed in dogs to circumvent immunological limitations, which might stand in our way in preclinical and clinical trials for DMD.

Materials and methods

Construction and production of rAAVs

We used rAAV2-CMVLacZ and rAAV2-CMVM3, which harbors the *LacZ* gene or microdystrophin M3 driven by the CMV promoter, respectively.[3,7,8] To improve the expression efficiency of the LacZ gene in rAAV2-CMVLacZ, a chimeric intron (human β-globin splicing donor and immunoglobulin splicing acceptor, Promega, Madison, WI, USA) is inserted between CMV promoter and the LacZ gene.[8] rAAV2-LacZ-P(−) was generated by deleting the truncated MCK promoter (358 bp) from rAAV2-MCKLacZ, leaving the MCK enhancer intact.[8] We confirmed that rAAV2-LacZ-P(−) could not express β-gal in murine muscle cells both *in vitro* and *in vivo* (data not shown). The rAAV was produced by a plasmid triple-cotransfection method,[23] purified by two CsCl density gradient centrifugations[24] and/or heparin column chromatography,[25] and titrated by a quantitative DNA dot-blot assay.

Administration of rAAVs into canine or murine skeletal muscles and isolation of the injected muscles

Experimental dogs were wild-type littermates of beagle-based CXMD$_J$ breeding colony at National Center of Neurology and Psychiatry (NCNP; Tokyo, Japan),[10,11] or golden retriever muscular dystrophy colony at Murdoch University (Perth, Australia).[26] All animals were cared and treated in accordance with the guidelines approved by Ethics Committee for Treatment of Laboratory Animals at NCNP or Animal Ethics Committee at Murdoch University, where three fundamental principles (replacement, reduction and refinement) were also considered. When a rAAV was injected into dogs, the animals were not vaccinated to relive influences of immune response by vaccination. rAAVs were injected intramuscularly at ages from 2 days to 14 months, and the muscles were isolated after 2, 4 and 8 weeks. Surgeries were done under anesthesia with isoflurane, as described previously.[27] Briefly, the ECU, tibialis anterior (TA) or EDL muscles were surgically exposed and two marker sutures were placed on the mid-belly of the muscle at proximal and distal positions apart approximately 20 mm. rAAV (5×10^{10}–8×10^{12} vg in 100 or 500 μl) or phosphate-buffered saline (PBS) was injected slowly into the muscles between two markers along the length. In biopsy and necropsy, the entire muscle blocks with two sutures were removed, divided into some pieces, and immediately frozen in isopentane precooled with liquid nitrogen. rAAV (5×10^{11} vg/50 μl) was also injected into TA muscles of C57BL/10 mice at 5 weeks, and the muscles were isolated at 2 or 4 weeks after the injection.

Immunosuppression

To suppress immune reaction, we treated rAAV-injected dogs with cyclosporine alone or cyclosporine combined with MMF for immunosuppression. Cyclosporine (NEORAL capsules; Novartis, Basel, Switzerland) was administrated orally at doses of 20–50 mg/kg/day and daily from −5 day of the injection. MMF (CellCept capsules, Roche Pharmaceuticals, Nutley, NJ, USA) was administrated orally at a dose of 30 mg/kg/day and daily from 0 day of the injection.

Histological and immunohistochemical analysis

Transverse cryosections from the rAAV-injected muscles were stained with H&E or 5-bromo-4-chloro-3-indolyl-β-D-galactopyranoside (X-Gal).[8]

Immunohistochemistry was performed as described previously.[8] Cryosections were incubated with the following antibodies: mouse monoclonal antibodies against canine CD4 (CA13.1E4, Serotec, Oxford, UK), canine CD8a (CA9.JD3, Serotec), canine CD11b (CA16.3E10, Serotec), canine B cells (CA2.1D6, Serotec), class I major histocompatibility antigen (H58A, VMRD, Pullman, WA, USA) and canine MHC class II (CA2.1C12, Serotec), and fluorescein-conjugated goat affinity-purified antibody to dog IgG (whole molecule) (Cappel, Solon, OH, USA). The primary antibodies were detected using VECTASTAIN ABC kit (Vector Laboratories, Burlingame, CA, USA), then visualized with diaminobenzidine, and counterstained with methyl green.

In vitro *infection assay in primary myotubes*

Canine or murine primary myoblasts were isolated and differentiated into myotubes, according to the previously published protocol[28] with some modifications. Briefly, muscle mass was removed from dogs or mice at 0 day to 2 weeks, weighted and minced. Cells were enzymatically dissociated in PBS (4 ml per g of tissue) containing dispase II (2.4 IU/ml, Godo Shusei, Tokyo, Japan) and Collagenase type XI (0.2%, Sigma, St Louis, USA), and 2.5 mM $CaCl_2$. The slurry was incubated at 37°C for 90–120 min with trituration every 15 min, and then passed through 100 μm pore mesh. The filtrate was spun at 350 *g*, and the pellet was resuspended in growth medium (F-10 medium with 20% fetal bovine serum (FBS) and 2.5 ng/ml human basic fibroblast growth factor (Sigma)). The cell suspension was then plated on non-coated dishes for 90 min, and non-adherent cells were collected and plated onto new dishes. After several repeats of this pre-plating procedure, myoblasts were enriched. To assess transduction efficiency of a rAAV in primary myotubes, the same numbers of myoblasts (2×10^4 cells/well) were plated onto 24-well plates and maintained for a few days in differentiation medium (Dulbecco's modified Eagle's medium with 5% FBS and 10 μg/ml human insulin (Sigma)), and then cultured in the presence of rAAV2-CMVLacZ (2×10^8–2×10^{11} vg/well), or co-infected with the rAAV2 and adenovirus Ad5-dlX[3]

(1×10^7 plaque-forming unit (PFU)/ml). After 2 days, cells were stained with X-Gal.

Quantification of rAAV genome in canine muscle

To quantify rAAV genomes, muscle sections were digested with proteinase K, followed by phenol/chloroform extraction and isopropanol precipitation. The DNA pellet was resuspended in TE buffer, and amplified by PCR with following primer sets: 5′-ccacgctgttttgacctccatag-3′ (downstream of transcription start site in the CMV promoter) and 5′-gtacaattccgcagcttttagagc-3′ (upstream of the *LacZ* gene) for rAAV2-CMVLacZ (the PCR product is 244 bp, illustrated in Figure 1a); 5′-gcagttatctggaagat cagg-3′ and 5′-cataaccaccacgctcatcg-3′ (within the *LacZ* gene) for rAAV2-LacZ-P(−) (the PCR product is 275 bp, illustrated in Figure 4a). As an internal control, the canine calmodulin gene II (CaMII; GenBank accession no. D12622) was amplified with following primers: 5′-gagaggactcatccaaggtcacac-3′ and 5′-tcagaaaccacggcat cagg-3′. AAV vector plasmids for rAAV2-CMVLacZ or rAAV2-LacZ-P(−) were served as a quantity control for standard amplification.

RT-PCR for transgene mRNAs

Total RNA was isolated from muscle sections using RNAqueous-Micro kit (Ambion, TX, USA). Then first-strand cDNA was synthesized using First-Strand cDNA Synthesis Kit (GE Healthcare UK Ltd, Buckinghamshire, UK). mRNA of rAAV2-CMVLacZ was detected using the same primers used for genomic DNA (Figure 1a). The amplified product is 178 bp. As an internal control glyceraldehyde-3-phosphate dehydrogenase mRNA (GenBank accession no. AB038240) was amplified using the following primer set: 5′-tcatctctgctccttctgctgat-3′ and 5′-ggctagaggagccaagcagtt-3′.

Western blot analysis

Muscle extracts were prepared from rAAV-injected canine muscles, separated on 7.5% sodium dodecyl sulfate-polyacrylamide gels, and then transferred onto polyvinylidene fluoride membranes, as described previously.[8] β-Gal protein was detected by rabbit polyclonal anti-β-gal antibody (Cappel).

ELISA

ELISA were performed as described previously.[8] The microtiter plate was precoated with β-gal, rAAV2-CMVLacZ or rAAV2-LacZ-P(−), incubated with the sera from dogs, and then reacted with a 1/5000 dilution of peroxidase-conjugated rabbit anti-dog IgG (whole molecule) (Sigma). Reactivity was determined by the color reaction of 3,3′,5,5′,-tetramethylbenzidine (TMBZ).

IFN-γ release assay

Spleen cells were isolated from C57BL/6 mice or beagle dogs, which were untreated with rAAVs. Splenetic cells were dissociated physically and passed through 100 μm filters. After removal of red blood cells using 0.83% ammonium chloride buffer (Sigma), splenocytes were cultured in RPMI medium containing 10% FBS at a density of 2×10^6 cells/well in 24-well plates for 2 days in the presence of various antigens: β-gal (500 ng to 50 μg), rAAV2-CMVLacZ (1×10^8–1×10^{10} vg), ConA (5 ng to 5 μg, GE Healthcare Bio-Science) and phytohemagglutinin (50 ng to 50 μg, Sigma). The supernatant of the culture was assayed for the secretion of IFN-γ using Mouse or Canine IFN-γ Quantikine ELISA Kit (R&D Systems, Minneapolis, MN, USA). The amounts of canine or murine IFN-γ were calibrated using recombinant canine or murine IFN-γ proteins as standards, respectively, according to manufacturer's instructions. Results are given as means with standard deviation (s.d.) of three experiments. Data were first evaluated by *F*-test. When equality of variances was shown, *t*-test was used to evaluate the statistical significance. When rejected, Aspin–Welch-test was used.

Acknowledgements

We are grateful to Dr Katsujiro Sato, Dr Yasushi Mochizuki, Dr Naoko Yugeta, Dr Akiyo Nishiyama, Dr Madoka Ikemoto, Dr Michiko Wada, Ms Kazue Kinoshita, Ms Ryoko Nakagawa, Mr Satoru Masuda, Dr Masayuki Tomohiro and Dr Yoshiki Shimatsu for technical assistance. We also thank Mr Hideki Kita and Mr Shinichi Ichikawa and other staff of JAC Co. for care and management of experimental animals. This work is supported by Grants-in-Aid for Scientific Research for Research on Nervous and Mental Disorders (10B-1, 13B-1, 16B-3) and Health Sciences Research Grants for Research on Human Genome and Gene Therapy (H10-genome-015, H13-genome-001, H16-genome-003) from the Ministry of Heath, Labor and Welfare of Japan, and Grant-in-Aid for Scientific Research (B) from the Ministry of Education, Culture, Sports, Science and Technology (MEXT). A part of this work in Musashino University is supported by High-Tech Research Center Project for Private Universities: matching fund subsidy from MEXT, 2004.

References

1 Emery AEH: *Duchenne Muscular Dystrophy*, 2nd edn. Oxford University Press: Oxford, 1993.
2 Fisher KJ, Jooss K, Alston J, Yang Y, Haecker SE, High K *et al.* Recombinant adeno-associated virus for muscle directed gene therapy. *Nat Med* 1997; **3**: 306–312.
3 Yuasa K, Miyagoe Y, Yamamoto K, Nabeshima Y, Dickson G, Takeda S. Effective restoration of dystrophin-associated proteins *in vivo* by adenovirus-mediated transfer of truncated dystrophin cDNAs. *FEBS Lett* 1998; **425**: 329–336.
4 Harper SQ, Hauser MA, Dellorusso C, Duan D, Crawford RW, Phelps SF *et al.* Modular flexibility of dystrophin: implications for gene therapy of Duchenne muscular dystrophy. *Nat Med* 2002; **8**: 253–261.
5 Watchko J, O'day T, Wang B, Zhou L, Tang Y, Li J *et al.* Adeno-associated virus vector-mediated minidystrophin gene therapy improves dystrophic muscle contractile function in *mdx* mice. *Hum Gene Ther* 2002; **13**: 1451–1460.
6 Fabb SA, Wells DJ, Serpente P, Dickson G. Adeno-associated virus vector gene transfer and sarcolemmal expression of a 144 kDa micro-dystrophin effectively restores the dystrophin-associated protein complex and inhibits myofibre degeneration in nude/*mdx* mice. *Hum Mol Genet* 2002; **11**: 733–741.
7 Sakamoto M, Yuasa K, Yoshimura M, Yokota T, Ikemoto T, Suzuki M *et al.* Micro-dystrophin cDNA ameliorates dystrophic phenotypes when introduced into *mdx* mice as a transgene. *Biochem Biophys Res Commun* 2002; **293**: 1265–1272.

8 Yuasa K, Sakamoto M, Miyagoe-Suzuki Y, Tanouchi A, Yamamoto H, Li J *et al.* Adeno-associated virus vector-mediated gene transfer into dystrophin-deficient skeletal muscles evokes enhanced immune response against the transgene product. *Gene Therapy* 2002; **9**: 1576–1588.
9 Yoshimura M, Sakamoto M, Ikemoto M, Mochizuki Y, Yuasa K, Miyagoe-Suzuki Y *et al.* AAV vector-mediated microdystrophin expression in a relatively small percentage of *mdx* myofibers improved the *mdx* phenotype. *Mol Ther* 2004; **10**: 821–828.
10 Shimatsu Y, Katagiri K, Furuta T, Nakura M, Tanioka Y, Yuasa K *et al.* Canine X-linked muscular dystrophy in Japan ($CXMD_J$). *Exp Animals* 2003; **52**: 93–97.
11 Shimatsu Y, Yoshimura M, Yuasa K, Urasawa N, Tomohiro M, Nakura M *et al.* Major clinical and histopathological characteristies of canine X-linked muscular dystrophy in Japan, $CXMD_J$. *Acta Myologica* 2005; **24**: 145–154.
12 Valentine BA, Cooper BJ, Cummings JF, De Lahunta A. Canine X-linked muscular dystrophy: morphologic lesions. *J Neurol Sci* 1990; **97**: 1–23.
13 Manno CS, Arruda VR, Pierce GF, Glader B, Ragni M, Rasko J *et al.* Successful transduction of liver in hemophilia by AAV-Factor IX and limitations imposed by the host immune response. *Nat Med* 2006; **12**: 342–347.
14 Fisher KJ, Gao GP, Weitzman MD, DeMatteo R, Burda JF, Wilson JM. Transduction with recombinant adeno-associated virus for gene therapy is limited by leading-strand synthesis. *J Virol* 1996; **70**: 520–532.
15 Herzog RW, Yang EY, Couto LB, Hagstrom JN, Elwell D, Fields PA *et al.* Long-term correction of canine hemophilia B by gene transfer of blood coagulation factor IX mediated by adeno-associated viral vector. *Nat Med* 1999; **5**: 56–63.
16 Fields PA, Kowalczyk DW, Arruda VR, Armstrong E, Mccleland ML, Hagstrom JN *et al.* Role of vector in activation of T cell subsets in immune responses against the secreted transgene product factor IX. *Mol Ther* 2000; **1**: 225–235.
17 Herzog RW, Mount JD, Arruda VR, High KA, Lothrop Jr CD. Muscle-directed gene transfer and transient immune suppression result in sustained partial correction of canine hemophilia B caused by a null mutation. *Mol Ther* 2001; **4**: 192–200.
18 Herzog RW, Fields PA, Arruda VR, Brubaker JO, Armstrong E, Mcclintock D *et al.* Influence of vector dose on factor IX-specific T and B cell responses in muscle-directed gene therapy. *Hum Gene Ther* 2002; **13**: 1281–1291.
19 Arruda VR, Stedman HH, Nichols TC, Haskins ME, Nicholson M, Herzog RW *et al.* Regional intravascular delivery of AAV-2-F.IX to skeletal muscle achieves long-term correction of hemophilia B in a large animal model. *Blood* 2005; **105**: 3458–3464.
20 Zhang Y, chirmule N, Gao G, Wilson J. CD40 ligand-dependent activation of cytotoxic T lymphocytes by adeno-associated virus vectors *in vivo*: role of immature dendritic cells. *J. Virol* 2000; **74**: 8003–8010.
21 Wang Z, Zhu T, Qiao C, Zhou L, Wang B, Zhang J *et al.* Adeno-associated virus serotype 8 efficiently delivers genes to muscle and heart. *Nat Biotechnol* 2005; **23**: 321–328.
22 Inagaki K, Fuess S, Storm TA, Gibson GA, Mctiernan CF, Kay MA *et al.* Robust systemic transduction with AAV9 vectors in mice: efficient global cardiac gene transfer superior to that of AAV8. *Mol Ther* 2006; **14**: 45–53.
23 Xiao X, Li J, Samulski RJ. Production of high-titer recombinant adeno-associated virus vectors in the absence of helper adenovirus. *J Virol* 1998; **72**: 2224–2232.
24 Snyder R, Xiao X, Samulski RJ. Production of recombinant adeno-associated viral vectors. In: Dracopoli N, Haines J, Korf B, Morton C, Seidman C, Seidman JG, Smith D (eds). *Current Protocols in Human Genetics*. John Wiley & Sons Ltd: New York, 1996, pp 12.1.1–12.2.23.
25 Auricchio A, Hildinger M, O'connor E, Gao GP, Wilson JM. Isolation of highly infectious and pure adeno-associated virus type 2 vectors with a single-step gravity-flow column. *Hum Gene Ther* 2001; **12**: 71–76.
26 Howell JM, Fletcher S, Kakulas BA, O'hara M, Lochmuller H, Karpati G. Use of the dog model for Duchenne muscular dystrophy in gene therapy trials. *Neuromuscul Disord* 1997; **7**: 325–328.
27 Howell JM, Lochmuller H, O'hara A, Fletcher S, Kakulas BA, Massie B *et al.* High-level dystrophin expression after adeno-virus-mediated dystrophin minigene transfer to skeletal muscle of dystrophic dogs: prolongation of expression with immuno-suppression. *Hum Gene Ther* 1998; **9**: 629–634.
28 Rando TA, Blau HM. Primary mouse myoblast purification, characterization, and transplantation for cell-mediated gene therapy. *J Cell Biol* 1994; **125**: 1275–1287.

Supplementary Information accompanies the paper on Gene Therapy website (http://www.nature.com/gt)

 Related Commentary, page 2388

NO production results in suspension-induced muscle atrophy through dislocation of neuronal NOS

Naoki Suzuki,[1,2] Norio Motohashi,[1] Akiyoshi Uezumi,[1] So-ichiro Fukada,[1] Tetsuhiko Yoshimura,[3] Yasuto Itoyama,[2] Masashi Aoki,[2] Yuko Miyagoe-Suzuki,[1] and Shin'ichi Takeda[1]

[1]Department of Molecular Therapy, National Institute of Neuroscience, National Center of Neurology and Psychiatry, Kodaira, Tokyo, Japan.
[2]Department of Neurology, Tohoku University School of Medicine, Seiryo-machi, Sendai, Japan.
[3]Project of Biofunctional Reactive Species, Yamagata Promotional Organization of Industrial Technology, Matsuei, Yamagata, Japan.

Forkhead box O (Foxo) transcription factors induce muscle atrophy by upregulating the muscle-specific E3 ubiquitin ligases MuRF-1 and atrogin-1/MAFbx, but other than Akt, the upstream regulators of Foxos during muscle atrophy are largely unknown. To examine the involvement of the dystrophin glycoprotein complex (DGC) in regulation of Foxo activities and muscle atrophy, we analyzed the expression of DGC members during tail suspension, a model of unloading-induced muscle atrophy. Among several DGC members, only neuronal NOS (nNOS) quickly dislocated from the sarcolemma to the cytoplasm during tail suspension. Electron paramagnetic resonance spectrometry revealed production of NO in atrophying muscle. nNOS-null mice showed much milder muscle atrophy after tail suspension than did wild-type mice. Importantly, nuclear accumulation of dephosphorylated Foxo3a was not evident in nNOS-null muscle, and neither MuRF-1 nor atrogin-1/MAFbx were upregulated during tail suspension. Furthermore, an nNOS-specific inhibitor, 7-nitroindazole, significantly prevented suspension-induced muscle atrophy. The NF-κB pathway was activated in both wild-type and nNOS-null muscle during tail suspension. We also show that nNOS was involved in the mechanism of denervation-induced atrophy. We conclude that nNOS/NO mediates muscle atrophy via regulation of Foxo transcription factors and is a new therapeutic target for disuse-induced muscle atrophy.

Introduction

Reduced muscle activity such as bed rest, limb immobilization, denervation, or unloading (e.g., tail suspension or space flight) leads to significant muscle atrophy (1, 2). In these conditions, the atrophying muscles show increased rates of protein degradation mainly through activation of the ubiquitin proteasome system (3, 4), and the muscle-specific E3 ubiquitin ligases muscle-specific RING finger protein 1 (MuRF-1) and atrogin-1/muscle atrophy F-box protein (atrogin-1/MAFbx) are commonly upregulated (3, 4). Recent studies further showed that muscle inactivity results in suppression of the IGF-1/PI3K/Akt pathway (5–8) and activation of transcription factors such as the forkhead box O (Foxo) family and NF-κB (9–11).

Foxo family of forkhead transcription factors regulates a variety of biological process such as metabolism, cell proliferation and death, tumor growth, response to stress, and longevity (12–15). Mammals have 4 members, Foxo1a, Foxo3a, Foxo4, and Foxo6 (12). Among them, Foxo1a is activated in almost all forms of muscle atrophy (16). Importantly, several experiments indicate that forced expression of Foxo1a or Foxo3a upregulates the expression of a variety of atrophy-related genes including MuRF-1 and atrogin-1/MAFbx genes and induces muscle atrophy both in vitro and in vivo (4, 10, 16, 17). These observations indicate that Foxo1a and Foxo3a are central players in atrophy signaling.

The activities of Foxo factors are thought to be regulated mainly at posttranslational levels by a serine/threonine kinase Akt. In the absence of muscle activities, Akt is inactivated, leading to dephosphorylation of Foxo transcription factors. As a result, dephosphorylated Foxos enter into the nucleus and activate atrophy-inducing genes (10, 18). Conversely, when Akt is activated, Foxos are phosphorylated and bound by 14-3-3 proteins and move from nucleus to cytoplasm (13, 19).

NF-κB is another key signaling molecule in muscle atrophy. In particular, crucial roles for NF-κB in both cachexia- and inactivity-induced muscle atrophy have been well investigated (9, 20, 21).

Several molecules are proposed as a mechanical sensor or a trigger of disuse atrophy. Recently it has been reported that muscles from tumor-bearing mice exhibited reduced levels of dystrophin, the protein that is mutated in Duchenne muscular dystrophy, together with reduced levels of dystrophin-associated glycoprotein (22, 23). Furthermore, forced expression of dystrophin in transgenic mice counteracted cachexia-induced muscle atrophy (22). The role of the dystrophin glycoprotein complex (DGC) in inactivity-induced muscle atrophy is not known yet, but these results raise the possibility that the DGC works as a regulator of muscle atrophy or serves as a scaffold for anti-atrophic signal transduction.

To clarify the roles for the DGC in muscle atrophy, we examined the expression and function of the members of DGC in skeletal muscle during tail suspension, a model of unloading. Here we demonstrate that neuronal NOS (nNOS), a peripheral member of the DGC, is activated in unloading conditions, regulates Foxo3a, and promotes muscle atrophy. We also show that a nNOS-specific

Nonstandard abbreviations used: DGC, dystrophin glycoprotein complex; EPR, electron paramagnetic resonance; Foxo, forkhead box O; IKKβ, inhibitor of NF-κB kinase β; L-NAME, N-nitro-L-arginine methylester; MAFbx, muscle atrophy F-box protein; MGD, *N*-methyl-D-glucamine-dithiocarbamate; mTOR, mammalian target of rapamycin; MuRF-1, muscle-specific RING finger protein 1; 7NI, 7-nitroindazole; nNOS, neuronal NOS.

Conflict of interest: The authors have declared that no conflict of interest exists.

Citation for this article: *J. Clin. Invest.* 117:2468–2476 (2007). doi:10.1172/JCI30654.

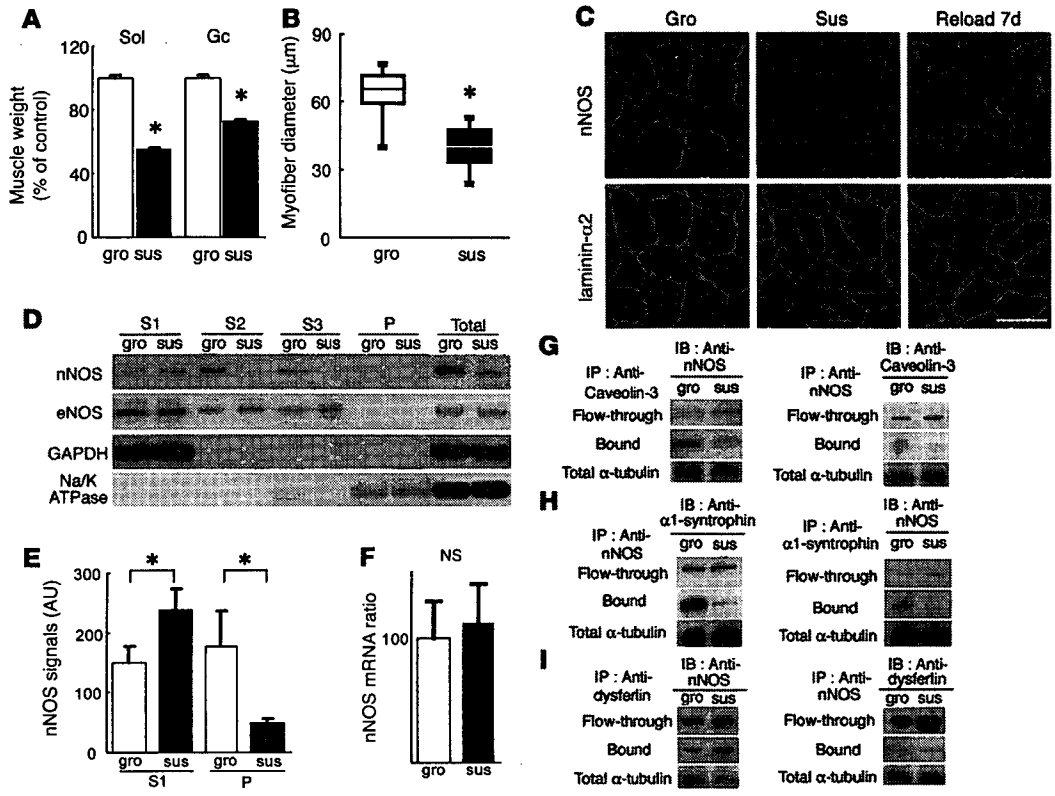

Figure 1

nNOS disappears from the sarcolemma during tail suspension. (**A**) Weights of soleus (Sol) and gastrocnemius (Gc) muscles from tail-suspended (sus) wild-type mice are normalized to body weight and are expressed as percentage of ground control (gro) (n = 15/group). *P < 0.05, Student's t test. (**B**) Box and whiskers plot of myofiber diameter size of soleus. Boxes represent the middle 50% of the data, lines represent the median, and whiskers represent the range. More than 200 fibers were measured on laminin-α2 chain–stained cross sections. (**C**) Immunofluorescent staining for nNOS and laminin-α2 chain. Transverse muscle sections from ground control mice, tail-suspended mice, and mice after reloading for 7 days (reload 7d) were stained with anti-nNOS (green) and anti–laminin-α2 chain antibodies (red). Scale bar: 50 μm. (**D**) Western blot using anti-nNOS antibody on subcellular fractions of muscle extracts. P indicates insoluble pellet after sequential extraction of skeletal muscle homogenates with 100 mM NaCl (S1), 500 mM NaCl (S2), and 0.5% Triton X-100 (S3). GAPDH signals in S1 and Na/K-ATPase signals in P confirmed that our fractionation was correctly done. Fractionation and western blotting were repeated 5 times, and representative data are presented. Note the slight increase of nNOS levels in S1 fraction and loss of nNOS signal in insoluble P fraction during tail suspension. (**E**) Quantification of nNOS signals in S1 and P fractions of muscle extracts shown in D (n = 5 /group). The signals in S1 and P fractions were normalized to GAPDH or Na/K-ATPase, respectively. Mann-Whitney, *P < 0.05. (**F**) Levels of nNOS mRNA in muscles from ground control mice and tail-suspended mice for 2 weeks were evaluated by real-time PCR (n = 5/group). No significant difference was found by Mann-Whitney test. (**G**) Immunoprecipitation with caveolin-3 antibody and immunoblot with nNOS antibody, and vice versa, for ground control and tail suspension groups. (**H**) Immunoprecipitation with α1-syntrophin Ab and immunoblot with nNOS antibody, and vice versa. (**I**) Immunoprecipitation of dysferlin antibody and immunoblot with nNOS Ab, and vice versa. In **G**–**I**, flow-through fraction was also examined by western blotting with anti–α-tubulin antibody.

inhibitor, 7-nitroindazole (7NI), significantly attenuates suspension-induced muscle atrophy. Furthermore, we show the involvement of nNOS in denervation-induced muscle atrophy process. Thus nNOS and NO are to our knowledge new therapeutic targets for disuse-induced muscle atrophy.

Results

nNOS disappears from the sarcolemma during tail suspension. To elucidate molecular mechanisms of unloading-induced muscle atrophy, we performed tail suspension (14 days) and reloading (7 days) experiments using wild-type C57BL/6 mice. The weights of the soleus and gastrocnemius (Figure 1A) muscles were decreased to 50%–70% of those of the control mice after tail suspension. The mice showed weakened grasping power and less endurance in running on the rotarod test after tail suspension (Supplemental Figure 1; supplemental material available online with this article; doi:10.1172/JCI30654DS1). The diameter of myofiber was also drastically decreased (Figure 1B). The expression patterns of the components of DGC, dystrophin, β-dystroglycan, α-sarcoglycan, dystrobrevin, laminin-α2, α1-syntrophin, and caveolin-3 were not changed during tail suspension (data not shown). The serum creatine kinase level was not elevated, and Evans blue dye uptake by myofibers was not evident in atrophied muscles (Supplemental Figure 2), indicating that the sarcolemmal integrity was maintained during tail suspension. nNOS mRNA levels were not significantly reduced (Figure 1F), and total nNOS protein was slightly decreased during tail suspension (Figure 1D). Importantly, immunohistochemistry revealed that nNOS was lost from the sarcolemma during tail suspension (Figure 1C). The sarcolemmal expression was gradually restored during the reloading process

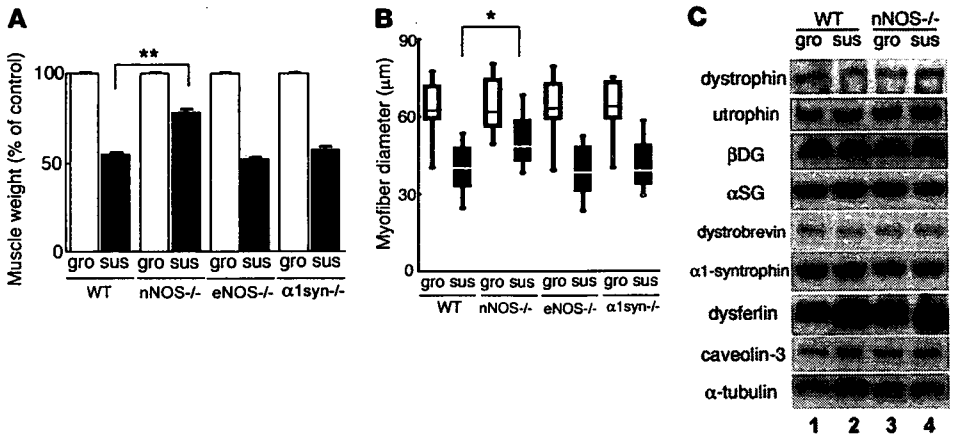

Figure 2

nNOS-null mice show partial tolerance to disuse-induced muscle atrophy. (**A**) Soleus muscle weight from ground control and tail-suspended wild-type ($n = 20$), nNOS-null ($n = 20$), eNOS-null ($n = 10$), and α1-syntrophin–null ($n = 10$) mice after 2-week tail suspension is shown as percent of wild-type ground controls. $^{**}P < 0.01$, Student's t test. (**B**) Box and whiskers plot of diameter of myofiber in soleus. Diameters were measured on H&E-stained cross sections of soleus muscles. $n = 200$ fibers in each experiment. $^{*}P < 0.05$, Student's t test. (**C**) Immunoblots of mouse gastrocnemius muscle extracts for DGC components from wild-type ground control (lane 1), wild-type tail-suspended (lane 2), nNOS-null ground control (lane 3), and nNOS-null tail-suspended (lane 4) mice. All lanes contain 30 μg of total protein. The experiments were performed 5 times, and representative pictures are presented.

(Figure 1C). eNOS expression was not changed (Figure 1D), and iNOS was not expressed (data not shown) during the course.

Next we performed subcellular fractionation of muscle homogenates as described previously (24). In ground control mice, nNOS remained in the insoluble pellet (Figure 1D). In tail-suspended mice, nNOS was largely extracted with 100 mM NaCl and barely detected in the pellet fraction (Figure 1D). Quantification of nNOS bands clearly showed that nNOS dislocated from the sarcolemma to the cytoplasm during tail suspension (Figure 1E). These results indicate that nNOS exists mainly in the cytoplasm during tail suspension. Immunoprecipitation experiments also revealed that nNOS completely dissociated from α1-syntrophin and caveolin-3 during tail suspension (Figure 1, G and H). In contrast, a considerable amount of dysferlin was immunoprecipitated with nNOS antibody during tail suspension (Figure 1I).

nNOS-null mice represent tolerance to disuse-induced muscle atrophy. To examine the roles of dislocated nNOS in muscle atrophy, we then performed tail suspension experiments using wild-type, nNOS-null, eNOS-null, and α1-syntrophin–null mice. The body weight (Figure 2A), average muscle fiber diameter (Figure 2B), and total number of muscle fibers (data not shown) of nNOS-null mice in the ground condition were similar to those of wild-type mice. However, after tail suspension for 14 days, reduction of muscle weight (Figure 2A), muscle size (Figure 2B), and muscle power (Supplemental Figure 1) were significantly less severe in the nNOS-null mice. Except for nNOS, dystrophin and other components of DGC were expressed in nNOS-null muscle at the same level as in wild-type muscle in both ground and suspended conditions (Figure 2C). eNOS-null muscle revealed atrophy during tail suspension similar to that seen in wild-type muscle (Figure 2, A and B), indicating that eNOS is not essential for atrophy signaling. We previously reported that disruption of the α1-syntrophin gene resulted in dislocation of nNOS from the sarcolemma to the cytoplasm without dystrophic phenotypes (25, 26). Suspension of α1-syntrophin–null mice induced severe muscle atrophy as it did in wild-type muscle (Figure 2, A and B).

Production of NO by nNOS in tail-suspended skeletal muscle. To directly measure the levels of NO in skeletal muscle during tail suspension, we employed electron paramagnetic resonance (EPR) spectrometry with *N*-methyl-D-glucamine-dithiocarbamate (MGD) and Fe^{2+} (27, 28). We injected MGD and Fe^{2+} into the wild-type and nNOS-null mice at the final stage of 2-week suspension, sacrificed the mice 30 minutes after the injection, and immediately measured the NO levels in muscle tissues. In EPR, the signal height, which is proportional to the amount of NO, was obtained by measuring the peak-to-peak height of the lower field side signal (arrow in Figure 3A) in the characteristic 3-line NO spectrum (29). NO levels in skeletal muscles increased during tail suspension, and the increase was inhibited by daily administration of 7NI to the mice. We used 50 mg/kg of 7NI to selectively inhibit nNOS (30, 31). The increase of NO levels in skeletal muscle during tail suspension was also inhibited by daily administration of 10 mg/kg of N-nitro-L-arginine methylester (L-NAME; pan-NOS inhibitor) (30) to the same extent (data not shown). NO levels in the skeletal muscle of nNOS-null mice after tail suspension were not different from those of ground control mice (Figure 3B), indicating that nNOS is mainly responsible for elevated levels of NO in muscle during tail suspension. Assay of the catalytic activity of NOS showed a higher level in the soluble (cytoplasmic) fraction than in the particulate fraction of suspended wild-type mice (Figure 3C).

Production of NO by nNOS is upstream of Foxo3a pathway. Foxo transcription factors are reported to upregulate many atrophy-related genes and promote muscle atrophy (9, 10). We found that Foxo3a was dephosphorylated and accumulated in the myonuclei of wild-type mice but not nNOS-null mice in western blotting (Figure 4, A and B) and in immunohistochemistry (Supplemental Figure 3). Foxo1 and Foxo4 were not changed during tail suspension in both wild-type and nNOS-null mice (Figure 4B). Recently, several groups have pointed out that the ubiquitin proteasome pathway is largely involved in selective protein degradation during the muscle atrophy process (3, 4). Consistent with this, mRNA levels of 2 muscle-specific E3 ubiquitin ligases, MuRF-1 and atrogin-1/MAFbx, increased during tail suspension in wild-type mice (Figure 4C) (9, 10). Remarkably, the upregulation of these E3 ligases was modest in nNOS-null mice. These observations suggest that nNOS regulates Foxo3a via NO production and thereby upregulates MuRF-1 and atrogin-1/MAFbx. To further examine whether nNOS regulates Foxo3a, we overexpressed nNOS in myotubes by a retrovirus vector (Supplemental Figure 4). Overexpressed nNOS increased both total and nuclear Foxo3a protein levels and decreased phosphorylated Foxo3a in myotubes (Supplemental Figure 4).

NF-κB pathway is activated during muscle atrophy in nNOS-null mice. NF-κB has been shown to be a major regulator of tail suspension–induced

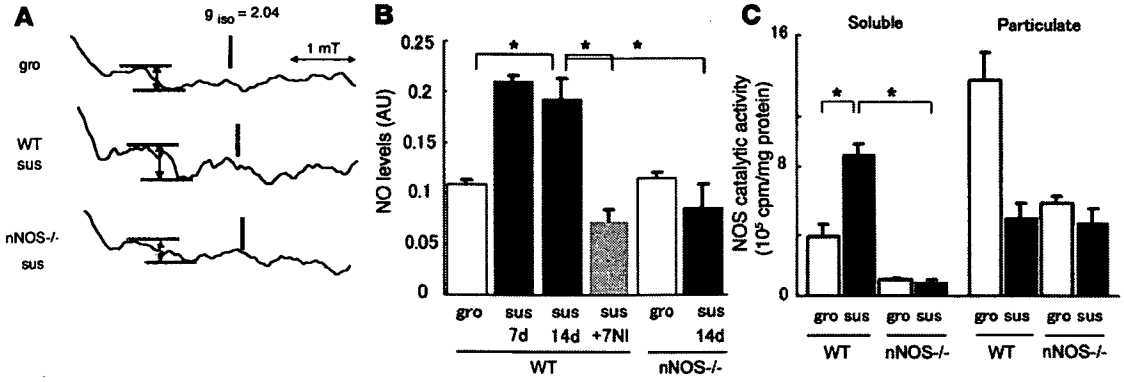

Figure 3

Measurement of NO in muscle and NOS activity during tail suspension. (**A**) EPR spectra of the NO adduct of Fe-MGD complex observed in skeletal muscle at room temperature. The NO-trapping agent was injected 30 minutes before measurements were taken. The EPR spectra of ground control and tail-suspended wild-type and nNOS-null mice were shown. Each spectrum represents the average of 5 accumulations. The signal height was obtained by measuring the peak-to-peak height of the lower field side signal (vertical arrows) in the 3-line spectrum. (**B**) NO levels of the skeletal muscle with and without tail suspension for 7 or 14 days were analyzed in EPR spectrometry ($n = 6$; $^*P < 0.05$, Mann-Whitney). Note that NO level in muscle is elevated in wild-type tail-suspended mice at 14 days but not in nNOS-null tail-suspended mice. 7NI was used as a selective nNOS inhibitor. (**C**) NOS catalytic activity in soluble and particulate fractions ($n = 5$; Mann-Whitney). [^{3}H]-citrulline, converted from [^{3}H]-arginine in vitro by NOS, was quantified by liquid scintillation spectroscopy. Note higher NOS activities in the soluble fraction than in the particulate fraction for suspended wild-type mice.

muscle atrophy (20, 21). EMSA showed that binding activity of NF-κB to its authentic binding sequence is increased by tail suspension in both wild-type and nNOS-null mice (Figure 4D). Importantly, there was no difference between tail-suspended wild-type and nNOS-null mice in the NF-κB binding activity (Figure 4D). In addition, western blotting revealed that p50 is increased by tail suspension (data not shown). These results suggest that NF-κB pathway was activated during tail suspension in the absence of nNOS. Whether the NF-κB activities mediate the residual muscle atrophy that occurred in nNOS-null mice during tail suspension remains to be clarified in a future study.

Inhibitor of NF-κB kinase β is nitrosylated during tail-suspension. Foxo3a is known to be phosphorylated by Akt in skeletal muscle (10, 18). In contrast to our expectation, there was no difference between wild-type and nNOS-null mice in the phosphorylation levels of Akt (Figure 5, A and B). There was no difference between the levels of S6k1 and mammalian target of rapamycin (mTOR), which are under regulation by PI3K/Akt signaling and positively regulate protein synthesis between wild-type and nNOS-null mice during tail suspension (5) (Figure 5A). A recent study reported that NO S-nitrosylates inhibitor of NF-κB kinase β (IKKβ) and thereby inhibits its activity (32). Other reports described inhibition of Foxo3a by IKKβ (33). Intriguingly, we found that tyrosine residues of IKKβ were nitrosylated during tail suspension in wild-type mice but not in nNOS-null mice (Figure 5C). However, whether S-nitrosylation of IKKβ detected during tail suspension contributes to activation of Foxo3a remains to be determined.

7NI alleviates tail suspension–induced muscle atrophy. To further examine the effect of inhibition of nNOS activity on muscle atrophy, 7NI, a nNOS-selective inhibitor, was injected daily into the peritoneal space of the wild-type mice during the 2-week tail suspension (Figure 6). This treatment significantly prevented muscle atrophy during tail suspension but did not increase muscle mass of ground control mice (Figure 6A). 7NI considerably increased phosphorylated Foxo3a and inhibited the increase in dephosphorylated and nuclear Foxo3a during tail suspension (Figure 6C). We also found that upregulation in mRNA levels of MuRF-1 and atrogin-1/MAFbx was abolished by 7NI during tail suspension (Figure 6B). These data imply that nNOS-specific inhibitor is a potential therapeutic strategy for disuse-induced muscle atrophy.

nNOS-null mice show milder muscle atrophy than wild-type mice after cutting of the sciatic nerve. We next examined the role of nNOS in denervation-induced muscle atrophy. Cutting the sciatic nerve on the denervated side resulted in greatly reduced muscle weight 14 days after operation (Figure 7A). Importantly, nNOS had already disappeared from the sarcolemma 3 days after denervation (Figure 7A). We observed much milder muscle atrophy in denervated muscle of nNOS-null mice than wild-type mice (Figure 7B), suggesting that nNOS is also involved in denervation-induced muscle atrophy. We then tested whether an nNOS inhibitor (7NI) or a pan-NOS inhibitor (L-NAME) counteracts denervation-induced muscle atrophy (Figure 7B). These 2 inhibitors limited the muscle atrophy (Figure 7B), indicating that NO is indeed a mediator and therefore a therapeutic target for denervation-induced muscle atrophy.

Discussion

Dislocation of nNOS is a major step in tail suspension–induced muscle atrophy. Involvement of the DGC in cachexia-induced muscle atrophy was recently reported (22). In our report, we demonstrate for what we believe to be the first time that nNOS is dislocated from the sarcolemma to the cytoplasm during tail suspension, whereas other members of the DGC are normally expressed at the sarcolemma. This observation implies that different mechanisms are involved in unloading-induced muscle atrophy and muscle atrophy seen in cachexia. Sarcolemmal nNOS is reported to be a versatile molecule that modulates satellite cell activation (34), formation of neuromuscular junction (35), glucose uptake (36), muscle contraction, and vasodilation (37). To clarify the mechanisms of nNOS translocation, we examined the effects of clenbuterol, streptomycin, and nifedipine on nNOS dislocation during tail suspension. After administration of these drugs, however, we still observed dislocation of nNOS during tail suspension (data not shown). These results suggest that sympathetic nerves, stretch-activated chan-

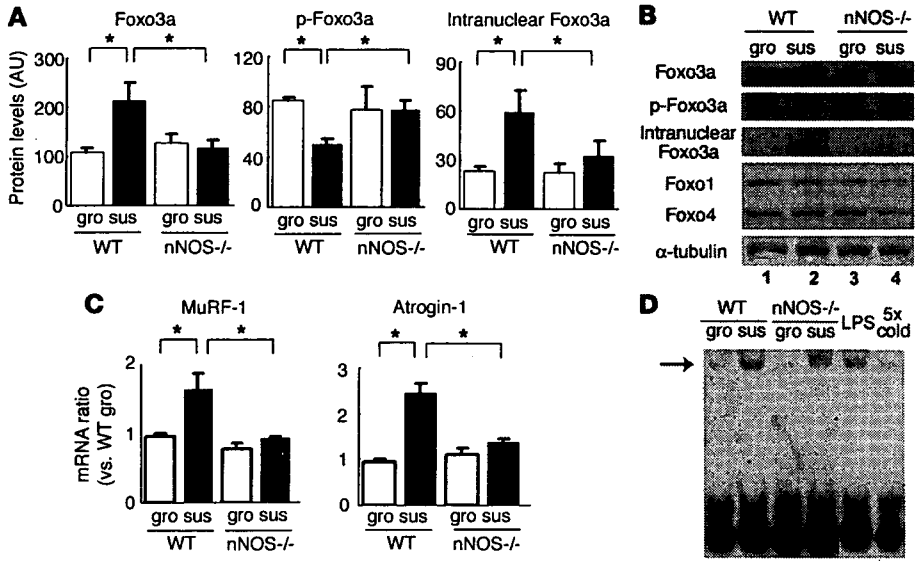

Figure 4

Participation of nNOS in regulation of Foxo3a and upregulation of MuRF-1 and atrogin-1/MAFbx. (**A**) The amounts of total Foxo3a, phosphorylated Foxo3a (p-Foxo3a), and intranuclear Foxo3a in wild-type and nNOS-null muscle during tail suspension were quantified (n = 5). Note that Foxo3a was dephosphorylated and accumulated in the myonuclei of wild-type mice but not of nNOS-null mice. *P < 0.05, Mann-Whitney. (**B**) Representative immunoblot analysis for Foxo3a, phosphorylated Foxo3a, Foxo1, and Foxo4 in total muscle extract, and Foxo3a in nuclear extracts in wild-type ground control (lane 1), wild-type tail-suspended (lane 2), nNOS-null ground control (lane 3), and nNOS-null tail-suspended (lane 4) muscles. α-Tubulin was used as a loading control. (**C**) mRNA levels of ubiquitin ligases (MuRF-1 and atrogin-1/MAFbx) (n = 5) were quantified by real-time RT-PCR. *P < 0.05, Mann-Whitney. (**D**) EMSA of NF-κB. Biotin-labeled double-stranded oligonucleotides containing NF-κB binding sites were incubated with nuclear extracts prepared from ground control and suspended muscles. An arrow indicates the DNA-protein complex. LPS was injected intraperitoneally into mice, and the muscle was used as a positive control for NF-κB binding activity. 5× cold, 5-fold excess of nonlabeled competitors.

nels, and L-type calcium channels are not involved in the dissociation of nNOS from the DGC.

nNOS is anchored at the sarcolemma by interaction with α1-syntrophin (25), a member of the DGC; interestingly, however, α1-syntrophin remains at the sarcolemma during tail suspension (data not shown). To examine whether modification of α1-syntrophin is involved in the dissociation of nNOS from α1-syntrophin, we performed 2-dimensional PAGE and western blotting with anti-α1-syntrophin antibody as previously described (38). The first dimensional isoelectric focusing reveals posttranslational modifications of α1-syntrophin. The results showed slight changes in mobility pattern of α1-syntrophin during tail suspension (data not shown), suggesting that some posttranslational modifications of α1-syntrophin may cause dissociation of nNOS from α1-syntrophin.

Dislocated nNOS leads to production of NO and regulates Foxo/E3 ubiquitin ligases pathway. EPR spectrometry confirmed that cytoplasmic nNOS led to production of NO during tail suspension (Figure 3, A and B). Tail suspension–induced muscle atrophy was blunted in nNOS-null mice (Figure 2, A and B) and 7NI-treated mice (Figure 6A) but not in eNOS-null mice (Figure 2, A and B). iNOS protein was not detected by western blotting in skeletal muscle during tail suspension (data not shown). These data indicate that dislocated nNOS, but neither eNOS nor iNOS, is involved in tail suspension–induced muscle atrophy.

We clearly show that 2 atrophy-related E3 ubiquitin ligases, MuRF-1 and atrogin-1/MAFbx, are not upregulated in nNOS-null muscle during tail suspension (Figure 4C and Figure 6B). Therefore, the induction of these genes is a downstream event of dislocation of nNOS in tail suspension-induced muscle atrophy.

Foxo transcription factors are reported to induce skeletal muscle atrophy by upregulating MuRF-1 or atrogin-1/MAFbx (4, 10, 16, 17). For example, transgenic mice overexpressing Foxo1 in skeletal muscle display a decrease in size of muscle fibers (17). Importantly, Foxo3a remained phosphorylated in nNOS-null mice during tail suspension, and total Foxo3a protein was not increased in tail-suspended nNOS null mice. Moreover, Foxo3a accumulated in the myonuclei of wild-type but not in nNOS-null mice during tail suspension (Figure 4B and Figure 6C).

When we overexpressed nNOS in muscle cells using a retrovirus vector, we found that Foxo3a was activated in nNOS-overexpressing myotubes (Supplemental Figure 4).

How does nNOS/NO regulate Foxo3a pathways? Our observations suggest that nNOS/NO is an upstream regulator of Foxo3a in the tail suspension-induced muscle atrophy process. There are at least 2 possible explanations for how Foxo3a regulates nNOS/NO. First, NO produced by nNOS might inhibit protein kinases, which phosphorylate Foxo3a, thereby protecting Foxo3a from degradation and promoting its translocation from the cytoplasm to the nucleus. There are several kinases that can phosphorylate Foxo, including Akt (10), IKKβ (33), BCR (39), and CDK2 (40). In the present study, we show that Akt activities in nNOS-null muscle were not different from those in wild-type muscle during tail suspension. A fraction of IKKβ was nitrosylated (inactivated) during tail suspension (Figure 5C), but NF-κB was activated in both wild-type and nNOS-null muscle during suspension. This observation suggests that IKKβ activity was not meaningfully disrupted (Figure 4D). Involvement of other kinases remains to be investigated in a future study.

Second, nNOS/NO signal might decrease nuclear export of Foxo3a, resulting in accumulation of Foxo3a in myonuclei and protecting it from phosphorylation by Akt. Foxo is exported from the nucleus in a 14-3-3 protein–dependent process (19), and these molecular interactions remain to be examined.

Dislocation of nNOS and production of NO have no obvious effects on the activity of NF-κB. It has been reported that reduced muscle activity induces muscle atrophy via activation of both Foxo and NF-κB transcription factors (9), at the same time suppressing the Akt pathway (5, 6), resulting in activation of the transcription of MuRF-1 and atrogin-1/MAFbx genes. In this report we demonstrated that dephosphorylation and nuclear accumulation of Foxo3a were largely attenuated in nNOS-null muscle during tail suspension. In contrast, our EMSA assay suggested that the NF-κB pathway was activated in nNOS-null

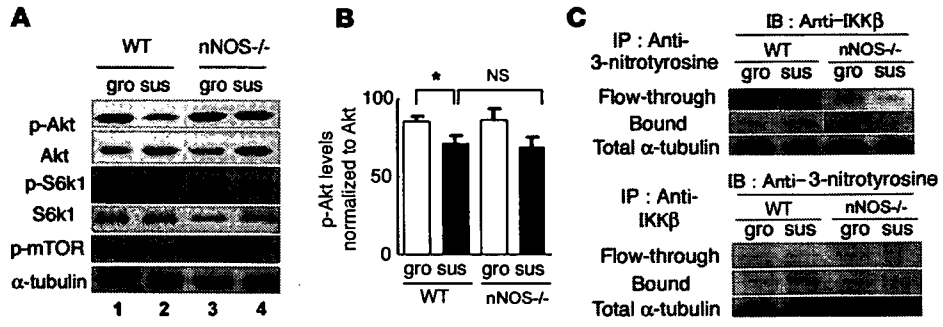

Figure 5

Phosphorylation of Akt and nitrosylation of IKKβ during 2-week tail suspension. (**A**) Immunoblots for protein synthesis pathway components (p-Akt, Akt, p-S6k1, S6k1, and p-mTOR) in wild-type ground control (lane 1), wild-type tail-suspended (lane 2), nNOS-null ground control (lane 3), and nNOS-null tail-suspended (lane 4) muscles. Densities of the bands were normalized to α-tubulin. (**B**) The ratio of phosphorylated Akt to total Akt is shown ($n = 5$; $^*P < 0.05$, Mann-Whitney). (**C**) Detection of nitrosylated IKKβ. Muscle proteins were immunoprecipitated with anti–3-nitrotyrosine antibody (upper panel) or with anti-IKKβ antibody (lower panel) and immunoblotted with anti-IKKβ or anti–3-nitrotyrosine antibodies, respectively. α-Tubulin signals in flow-through fractions are also shown.

mice to a similar extent as in wild-type mice in tail suspension experiments. This observation raises the possibility that NF-κB mediated the residual atrophy that occurred in nNOS-null mice, but further investigation is needed to correctly answer this question.

nNOS and other muscle atrophies. Many conditions induce muscle atrophy, including space flight, immobilization, denervation, cancer cachexia, motor neuron diseases, starvation, and aging (41). Recently it has been reported that muscles of tumor-bearing mice exhibited membrane abnormalities accompanied by reduced levels of dystrophin and increased glycosylation on DGC proteins (22, 23). It was also shown that the DGC could counteract atrophic signaling in cancer cachexia when overexpressed at the sarcolemma (22). In the tail suspension model, we observed dislocation of nNOS but no changes in the sarcolemmal expression of other members of the DGC (Figure 2C). Therefore it is possible that dystrophin deficiency in cancer cachexia induces nNOS dislocation, which results in activation of nNOS and its downstream effectors.

We also found nNOS dislocation in denervation-induced muscle atrophy (Figure 7A). Remarkably, denervation-induced muscle atrophy was modestly blunted in nNOS-null mice or selective nNOS inhibitor–treated mice (Figure 7B). Although iNOS was induced during denervation (data not shown), both 7NI and L-NAME showed a similar effect on muscle atrophy, suggesting that iNOS does not contribute to denervation-induced muscle atrophy.

In conclusion, we demonstrate that nNOS dislocated from the sarcolemma to the cytoplasm in 2 models of disuse-induced muscle atrophy, tail suspension and denervation. We also show that dislocated nNOS led to the production of NO and regulated Foxo3a, MuRF-1, and atrogin-1/MAFbx, key molecules in muscle atrophy. Our model is illustrated in Figure 8. The identification of nNOS as a regulator of unloading-induced muscle wasting suggests that pharmacological intervention targeting nNOS or its downstream or upstream pathways would prevent or diminish this debilitating process.

Methods

Animals and tail suspension model. Twelve-week-old female C57BL/6, nNOS-null and eNOS-null mice were purchased from the Jackson Laboratory. α1-Syntrophin-null mice were produced in our previous study (25). These mice were backcrossed to the C57BL/6 strain for more than 10 generations. The animals were allowed ad libitum access to food and drinking water. The Experimental Animal Care and Use Committee of the National Institute of Neuroscience approved all experimental protocols. The mice were randomly assigned to control or tail suspension groups. To induce muscle atrophy by disuse, mice were suspended so that their hind limbs were 1 mm off the cage floor for 14 days. After 14 days of tail suspension, some groups were allowed 7 days of reloading by normal weight bearing. Muscle weight was normalized to body weight and is presented as a percentage of control in each experiment.

Denervation model. The left sciatic nerve of mice was excised for nearly the full length of the thigh (approximately 10 mm) from a small incision (approximately 4 mm) made in the mid-lateral thigh under general anesthesia under a surgical microscope (Olympus) (42). The mice were sacrificed 3 or 14 days after denervation by cervical dislocation under general anesthesia, and soleus and gastrocnemius muscles were excised for analysis. The right gastrocnemius muscle served as a control.

Reagents. Lipopolysaccharide from *E. coli* (0.1 ml, 3 mg/kg; *E. coli*, serotype 055:B5; Sigma-Aldrich) was administered via intraperitoneal injection. 7NI (Dojindo) was dissolved in peanut oil (50 mg/kg). L-NAME was injected daily into the intraperitoneal cavity of mice (10 mg/kg body weight). Clenbuterol (1 mg/kg; Sigma-Aldrich), streptomycin (300 mg/kg; Sigma-Aldrich) and nifedipine (5 mg/kg; Wako) were dissolved in PBS. PBS was injected into control mice.

Tissue preparation. Control and tail-suspended mice were sacrificed with cervical dislocation. Body and wet muscle were weighed. The gastrocnemius and soleus muscles were collected individually using standard dissection methods and cleaned of excess fat, connective tissue, and tendons. Several of the muscles were frozen in isopentane cooled by liquid nitrogen for histological and immunohistochemical analysis, and the other muscles were frozen directly in liquid nitrogen for RNA isolation or protein extraction and stored at -80°C.

Real time PCR. Total RNA was isolated using TRIzol (GIBCO). For RT-PCR, first-strand cDNA was synthesized using oligo-dT primers. Expression levels of selected genes (nNOS, MuRF-1, atrogin-1/MAFbx, and 18S-rRNA) were analyzed using Applied Biosystems SYBR Green gene expression assays on ABI7700 Sequence Detection System (Applied Biosystems) following the manufacturer's instructions.

H&E staining. Ten-micrometer cryosections were cut in the middle part of the muscle belly to obtain the largest myofiber diameter, placed on poly-L-lysine–coated slides, air dried, and stained with H&E. The sections were viewed and photographed using an HC-2500 digital camera system (Fuji Photo Film).

Immunohistochemistry. Cryostat sections of muscle tissue (10 μm thick), were postfixed in acetone or 4% paraformaldehyde at -20°C and preincubated in PBS containing 5% goat serum and 1% bovine serum albumin for 30 minutes at room temperature. Polyclonal anti-nNOS (Zymed), anti-Foxo3a (Sigma-Aldrich), and anti-laminin-α2 (Alexis) were applied overnight at 4°C. Following incubations with appropriate secondary antibodies, mounted sections were observed by using a Leica confocal microscope. Muscle fiber diameters were determined on cross sections of soleus muscle using the greatest distance between the oppo-

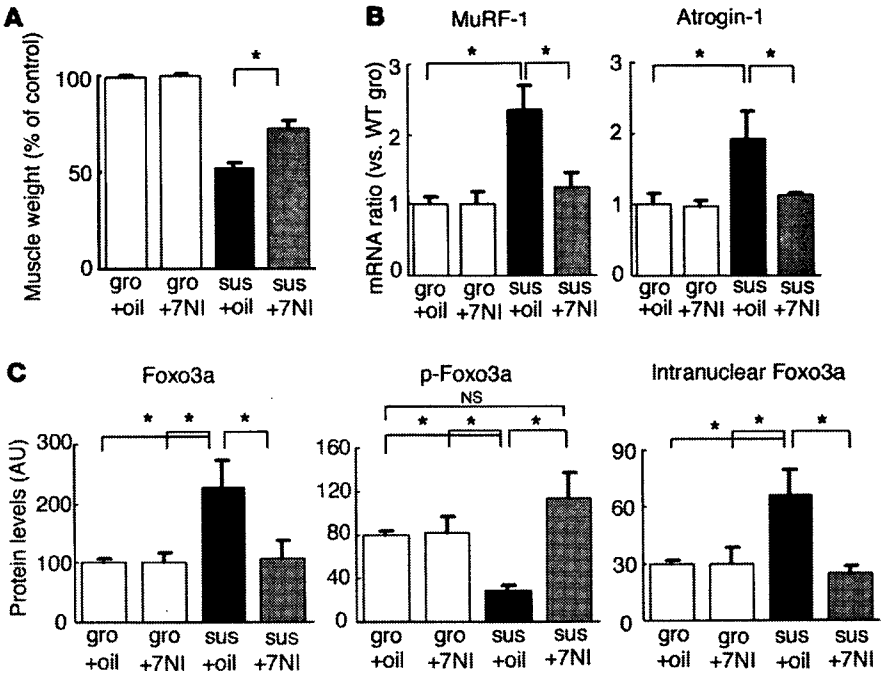

Figure 6
7NI alleviates muscle atrophy during ta suspension. (**A**) Soleus muscle weight (wild-type ground control and wild-type tai suspended mice with (+7NI) or without 7N (+oil). Oil or 7NI (50 mg/kg/d) was injecte daily into the abdominal cavity of the mic during 2-week tail suspension. Values (mus cle weight/body weight) are expressed a percent of wild-type oil-injected muscles afte 14-day tail suspension (n = 5–10 per grou; $^*P < 0.05$, Mann-Whitney). (**B**) mRNA lev els of MuRF-1 and atrogin-1/MAFbx (n = 4 in muscle from wild-type ground control an wild-type tail-suspended mice with or witho 7NI were quantified by real-time RT-PCI ($^*P < 0.05$, Mann-Whitney). (**C**) The amour of total Foxo3a, dephosphorylated Foxo3 and intranuclear Foxo3a (n = 4) were ana lyzed by western blotting, and band dens ties were normalized to α-tubulin ($^*P < 0.0$ Mann-Whitney).

site sides of the narrowest aspect of the fiber. Total number of muscle fibers was also counted on cross sections.

Western blotting. Total skeletal muscle protein was extracted from mouse hindlimb muscle for western blot analysis. We used the Bradford method and Coomassie Brilliant Blue G-250 (Bio-Rad) to determine the protein concentrations. Then protein fractions were extracted with a reducing sample buffer containing 10% SDS, 70 mM Tris-HCl, 5% β-mercaptoethanol, and Complete inhibitor cocktail (Roche). Protein (15 or 30 μg per lane) was separated on an SDS-polyacrylamide gel. The resulting gel was subsequently transferred to a polyvinylidene difluoride membrane (Millipore) using 242 mA for 1 hour. The blot was later incubated with primary antibodies. The signals were detected using the enhanced chemiluminescence method (GE Amersham). Relative quantities of proteins in western blo were determined by scanning densitometry (Alpha Innotec) and expresse in arbitrary units. The following antibodies were used for immunoblottin anti-α1-syntrophin (Biogenesis), anti-laminin-α2 (Alexis), anti-dystrophi (dys2), anti-utrophin, anti-β-dystroglycan, anti-dystrobrevin, anti-dysfe lin, anti-caveolin-3 (Novocastra), anti-hsp90 (Stressgen), anti-nNOS, ant IKKβ, anti-Akt, anti-p-Akt, anti-p-mTOR, anti-p50 (Transduction Labo ratories), anti-Foxo3a, anti-p-Foxo3a, anti-Foxo1/4, anti-Na/K-ATPas (Upstate Biotechnology), anti-Hsp70, and anti-iNOS antibody (Santa Cru Biotechnology Inc.). Anti-α-sarcoglycan antibody was kindly provided b Michihiro Imamura (National Institute of Neuroscience, National Cent of Neurology and Psychiatry).

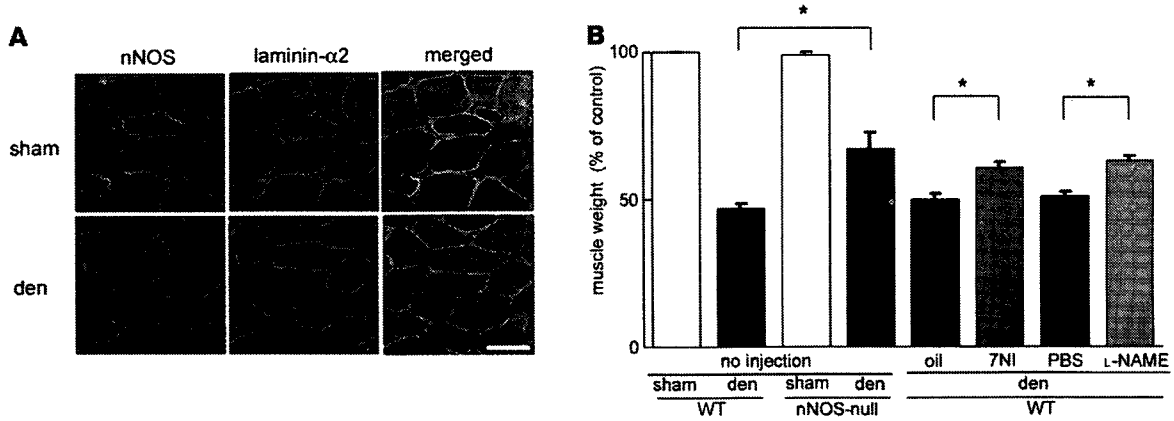

Figure 7
Inhibition of nNOS activities counteracts denervation-induced muscle atrophy. (**A**) Sarcolemmal expression of nNOS in control and denervate muscles. Transverse muscle sections from denervated (den) and sham-operated mice were stained with anti-nNOS (green) and anti-laminin-α chain (red) antibodies 3 days after sciatic nerve excision. Scale bar: 50 μm. (**B**) Reduction in soleus muscle weight of wild-type and nNOS-nu mice 2 weeks after sham operation or denervation. Weight of wild-type denervated muscle was also measured after 2-week administration of c 7NI, PBS, or L-NAME. Values (muscle weight/body weight) were expressed as percentage of the values of sham-operated wild-type muscl (n = 5–10 per group). $^*P < 0.05$, Mann-Whitney.

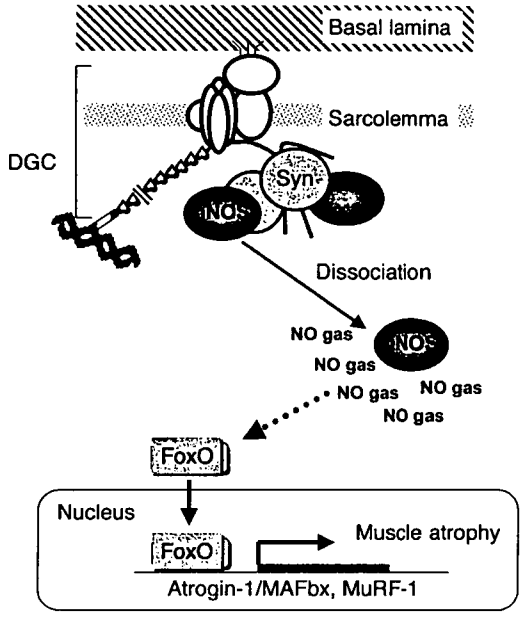

Figure 8
A model of nNOS involvement in tail suspension–induced muscle atrophy. Under normal conditions nNOS is located at the sarcolemma as a peripheral member of the DGC. During tail suspension, nNOS dissociates from α1-sytrophin (syn) and dislocates into the cytoplasm, generating NO, which ultimately regulates Foxo transcription factors, and muscle-specific E3 ubiquitin ligases, MuRF-1, and atrogin-1/MAFbx, which promote muscle protein degradation by the ubiquitin-proteasome system.

Nuclear and cytosolic protein extraction. Nuclear extracts were prepared from mouse skeletal muscle according to the method of Hunter et al. (20). Briefly, the cytosolic extract was obtained from the first supernatant of the nuclear extract preparation. The supernatant was placed in Millipore Ultrafree-4 centrifugal columns that had been pre-wetted with 0.5 ml of dilution buffer (20 mM HEPES, 40 mM KCl, 10% glycerol, 0.2 mM EDTA, 1 mM DTT), and centrifuged (7,500 *g*) at 4°C for 30 minutes. Dilution buffer (0.8 ml) was added to the column, and the 30-minute spin was repeated. Protein concentrations were determined using the Bradford protein assay (Bio-Rad).

Immunoprecipitation. Skeletal muscle samples were homogenized in 0.15 M NaCl, 10 mM HEPES (pH 7.5) and Complete inhibitor cocktail (Roche), with or without 1% digitonin (Wako). nNOS and caveolin-3 immunoprecipitation was performed with anti-nNOS goat polyclonal antibody (Santa Cruz Biotechnology Inc.) and anti-caveolin-3 antibody (Transduction Laboratories). The samples were incubated with protein G gel (GE Amersham) overnight at 4°C. After the gel was washed with the equilibrating buffer, the bound fraction was eluted with 1% SDS, 1 mM tris-(2-carboxyethyl) phosphine, and 14 mM Tris-HCl (pH 6.7) and concentrated. Coimmunoprecipitates were resolved by SDS-PAGE and analyzed by western blotting. α-Tubulin was used as internal control for total protein inputted.

Two-dimensional PAGE. Muscle extracts from ground control and tail suspension mice were resolved on 2-dimensional PAGE and analyzed by western blotting as described in ref. 38.

EMSA. EMSA was performed according to the manufacturer's instructions (Panomics). Briefly, probes were end-labeled with biotin. Binding reactions were performed for 30 minutes in a volume of 10 ml. Specificity of DNA binding was determined by addition of a 5-fold molar excess of unlabeled competitor DNA to the binding reactions. The binding reactions were loaded onto 6% non-denaturing polyacrylamide gels and electrophoretically resolved in 0.5× tris-borate EDTA (TBE) buffer.

NOS catalytic assays. NOS catalytic assays were carried out according to the method described by Brenman et al. (24). Muscles from wild-type and nNOS-null mice with or without tail suspension were homogenized in 10 volumes of buffer containing 25 mM Tris-HCl, pH 7.4, 1 mM EDTA, 1 mM EGTA, and 0.1 mM NaCl. The homogenate was centrifuged at 20,000 *g* to separate the soluble fraction. The pellet was extracted in the same buffer containing 0.5 M NaCl and centrifuged at 20,000 *g* to create a particulate fraction. Aliquots from these fractions were assayed in 125-μl reactions containing 1.8×10^5 cpm of [^{3}H]-arginine (53.0 Ci/mmol; GE Amersham), 1 mM NADPH, 640 μM $CaCl_2$, 1 μM calmodulin, and 3 μM each of tetrahydrobiopterin, FAD, and FMN. After incubation for 20 minutes at 37°C, the assays were terminated with 2 ml of 20 mM HEPES, pH 5.5, and 2 mM EDTA. The samples were then applied to AG50WX-8 columns (Na^+ form; Dowex), which were centrifuged, and the supernatant was collected. [^{3}H]-citrulline was quantified by liquid scintillation spectroscopy.

Subcellular fractionation. The subcellular fractionation was performed according to the method described by Brenman et al. (24). The gastrocnemius muscle was homogenized in 10 volumes (w/v) of buffer A (25 mM Tris-HCl, pH 7.4, 100 mM NaCl, 1 mM EDTA, 1 mM EGTA). The nuclei of the muscle were pelleted by centrifugation at 1,000 *g*. The supernatant was then centrifuged at 20,000 *g* to yield the supernatant S1. The resulting heavy microsomal pellet was resuspended in buffer B (500 mM NaCl added to buffer A), incubated for 30 minutes at 4°C with agitation, and centrifuged at 15,000 *g*, yielding supernatant S2. The pellet from this last centrifugation was resuspended in buffer B containing 0.5% Triton X-100, incubated for 30 minutes at 4°C with agitation, and centrifuged at 15,000 *g* to create supernatant S3 and the final pellet. The fractions were resolved using the sample buffer and analyzed by SDS-polyacrylamide gel electrophoresis. The proteins were transferred to a polyvinylidene difluoride membrane (Millipore), which was later incubated with anti-nNOS antibody. The bands were quantified in densitometry.

Direct measurement of NO by EPR spectrometry. Concentrations of NO in the skeletal muscle of mice were measured using the NO-trapping technique combined with EPR spectroscopy (29). Spin traps react with unstable free radicals such as NO to form a relatively stable radical adduct. This long-lived adduct formation results in accumulation of a steady-state formation of these free radicals, and thus the resultant radical adduct can be detected readily by EPR spectroscopy. We used a Fe-MGD complex as the trapping agent to quantify NO levels in the skeletal muscle tissues of the mice. Solutions of $FeSO_4$ (62 mg/kg; Wako) and MGD (348 mg/kg; Dojindo) were injected subcutaneously. The Fe-MGD complex formed had a high specificity for NO (27, 29), and the NO-Fe-MGD complex was detected by EPR spectroscopy. The amplitude of the signal measured from the peak-to-peak height of the lower field side signal in the 3-line spectrum is known to be proportional to the amount of NO (29). The level of NO-Fe-MGD complex was estimated by comparing it with the signal height of a standard solution of a chemically synthesized NO complex. The concentration in tissues was determined 30 minutes after injection of the NO-trapping reagent. Thirty minutes after administration of the reagent, the gastrocnemius and soleus muscle were removed and weighed (approximately 100–120 mg). The tissue was minced and subjected to immediate measurement of NO by EPR spectrometry. X-band EPR spectra were measured at room temperature with a TE-200 EPR spectrometer (JEOL). The homogenates were drawn into a capillary tube (75 mm in length, 46 μl in internal volume) that had been inserted first into an EPR quartz tube (outside diameter, 5 mm), then introduced into the cavity. The instrument settings were as follows: center field, 331 mT; field scan, 4 mT; sweep time, 2 min; time

constant, 0.3 s; modulation amplitude, 0.32 mT; modulation frequency, 9.44 GHz; microwave power, 60 mW.

Statistics. Statistical differences were determined by either 2-tailed unpaired Student's *t* test or the Mann-Whitney test. All data are expressed as mean ± SEM. Statistical significance is defined as $P < 0.05$.

Acknowledgments

We thank S. Masuda, A. Fukase, and T. Harano for technical support; K. Asanuma and J. Yoshitake for EPR spectrometry; Y. Onodera and M. Tateyama for immunohistochemistry; and all members of the Department of Molecular Therapy, National Institute of Neuroscience, for technical assistance and useful discussion, especially M. Yoshida, M. Ikemoto, and Y. Mochizuki. We also thank K. Ono for correcting our English. This work was supported by Research on Nervous and Mental Disorders (grant 16B-2); Health Science Research Grants for research on the human genome and gene therapy (H16-genome-003) and for research on brain science (H15-kokoro-021 and H18-kokoro-019) from the Japanese Ministry of Health, Labor and Welfare; Grants-in-Aid for Scientific Research (14657158, 15390281, 16590333, 17590857, and 18590392) from the Japanese Ministry of Education, Culture, Sports, Science and Technology; and the Ground-based Research Program for Space Utilization, promoted by Japan Space Forum.

Received for publication October 16, 2006, and accepted in revised form May 29, 2007.

Address correspondence to: Shin'ichi Takeda, Department of Molecular Therapy, National Institute of Neuroscience, National Center of Neurology and Psychiatry, 4-1-1 Ogawa-higashi, Kodaira, Tokyo 187-8502, Japan. Phone: 81-42-346-1720; Fax: 81-42-346-1750; E-mail: takeda@ncnp.go.jp.

1. Tidball, J.G. 2005. Mechanical signal transduction in skeletal muscle growth and adaptation. *J. Appl. Physiol.* **98**:1900–1908.
2. Ikemoto, M., et al. 2001. Space shuttle flight (STS-90) enhances degradation of rat myosin heavy chain in association with activation of ubiquitin-proteasome pathway. *FASEB J.* **15**:1279–1281.
3. Bodine, S.C., et al. 2001. Identification of ubiquitin ligases required for skeletal muscle atrophy. *Science.* **294**:1704–1708.
4. Gomes, M.D., Lecker, S.H., Jagoe, R.T., Navon, A., and Goldberg, A.L. 2001. Atrogin-1, a muscle-specific F-box protein highly expressed during muscle atrophy. *Proc. Natl. Acad. Sci. U. S. A.* **98**:14440–14445.
5. Bodine, S.C., et al. 2001. Akt/mTOR pathway is a crucial regulator of skeletal muscle hypertrophy and can prevent muscle atrophy in vivo. *Nat. Cell Biol.* **3**:1014–1019.
6. Song, Y.H., et al. 2005. Muscle-specific expression of IGF-1 blocks angiotensin II-induced skeletal muscle wasting. *J. Clin. Invest.* **115**:451–458. doi:10.1172/JCI200522324.
7. Rommel, C., et al. 2001. Mediation of IGF-1-induced skeletal myotube hypertrophy by PI(3)K/Akt/mTOR and PI(3)K/Akt/GSK3 pathways. *Nat. Cell Biol.* **3**:1009–1013.
8. Latres, E., et al. 2005. Insulin-like growth factor-1 (IGF-1) inversely regulates atrophy-induced genes via the phosphatidylinositol 3-kinase/Akt/mammalian target of rapamycin (PI3K/Akt/mTOR) pathway. *J. Biol. Chem.* **280**:2737–2744.
9. Cai, D., et al. 2004. IKKbeta/NF-kappaB activation causes severe muscle wasting in mice. *Cell.* **119**:285–298.
10. Sandri, M., et al. 2004. Foxo transcription factors induce the atrophy-related ubiquitin ligase atrogin-1 and cause skeletal muscle atrophy. *Cell.* **117**:399–412.
11. Li, Y.P., Schwartz, R.J., Waddell, I.D., Holloway, B.R., and Reid, M.B. 1998. Skeletal muscle myocytes undergo protein loss and reactive oxygen-mediated NF-kappaB activation in response to tumor necrosis factor alpha. *FASEB J.* **12**:871–880.
12. Greer, E.L., and Brunet, A. 2005. FOXO transcription factors at the interface between longevity and tumor suppression. *Oncogene.* **24**:7410–7425.
13. Lehtinen, M.K., et al. 2006. A conserved MST-FOXO signaling pathway mediates oxidative-stress responses and extends life span. *Cell.* **125**:987–1001.
14. Matsumoto, M., Han, S., Kitamura, T., and Accili, D. 2006. Dual role of transcription factor FoxO1 in controlling hepatic insulin sensitivity and lipid metabolism. *J. Clin. Invest.* **116**:2464–2472. doi:10.1172/JCI27047.
15. Berman, J., and Kenyon, C. 2006. Germ-cell loss extends C. elegans life span through regulation of DAF-16 by kri-1 and lipophilic-hormone signaling. *Cell.* **124**:1055–1068.
16. Lecker, S.H., et al. 2004. Multiple types of skeletal muscle atrophy involve a common program of changes in gene expression. *FASEB J.* **18**:39–51.
17. Kamei, Y., et al. 2004. Skeletal muscle FOXO1 (FKHR) transgenic mice have less skeletal muscle mass, down-regulated Type I (slow twitch/red muscle) fiber genes, and impaired glycemic control. *J. Biol. Chem.* **279**:41114–41123.
18. Skurk, C., et al. 2005. The FOXO3a transcription factor regulates cardiac myocyte size downstream of AKT signaling. *J. Biol. Chem.* **280**:20814–20823.
19. Obsilova, V., et al. 2005. 14-3-3 Protein interacts with nuclear localization sequence of forkhead transcription factor FoxO4. *Biochemistry.* **44**:11608–11617.
20. Hunter, R.B., et al. 2002. Activation of an alternative NF-kappaB pathway in skeletal muscle during disuse atrophy. *FASEB J.* **16**:529–538.
21. Hunter, R.B., and Kandarian, S.C. 2004. Disruption of either the Nfkb1 or the Bcl3 gene inhibits skeletal muscle atrophy. *J. Clin. Invest.* **114**:1504–1511. doi:10.1172/JCI200421696.
22. Acharyya, S., et al. 2005. Dystrophin glycoprotein complex dysfunction: A regulatory link between muscular dystrophy and cancer cachexia. *Cancer Cell.* **8**:421–432.
23. Acharyya, S., et al. 2004. Cancer cachexia is regulated by selective targeting of skeletal muscle gene products. *J. Clin. Invest.* **114**:370–378. doi:10.1172/JCI200420174.
24. Brenman, J.E., Chao, D.S., Xia, H., Aldape, K., and Bredt, D.S. 1995. Nitric oxide synthase complexed with dystrophin and absent from skeletal muscle sarcolemma in Duchenne muscular dystrophy. *Cell.* **82**:743–752.
25. Kameya, S., et al. 1999. Alpha1-syntrophin gene disruption results in the absence of neuronal-type nitric-oxide synthase at the sarcolemma but does not induce muscle degeneration. *J. Biol. Chem.* **274**:2193–2200.
26. Hosaka, Y., et al. 2002. Alpha1-syntrophin-deficient skeletal muscle exhibits hypertrophy and aberrant formation of neuromuscular junctions during regeneration. *J. Cell Biol.* **158**:1097–1107.
27. Lecour, S., et al. 2001. Levels of nitric oxide in the heart after experimental myocardial ischemia. *J. Cardiovasc. Pharmacol.* **37**:55–63.
28. Asanuma, K., et al. 2005. Diffusion of cytotoxic concentrations of nitric oxide generated luminally at the gastro-oesophageal junction of rats. *Gut.* **54**:1072–1077.
29. Nagano, T., and Yoshimura, T. 2002. Bioimaging of Nitric Oxide. *Chem. Rev.* **102**:1235–1270.
30. Kato, N., Sato, S., Yokoyama, H., Kayama, T., and Yoshimura, T. 2005. Sequential changes of nitric oxide levels in the temporal lobes of kainic acid-treated mice following application of nitric oxide synthase inhibitors and phenobarbital. *Epilepsy Res.* **65**:81–91.
31. Moore, P.K., and Bland-Ward, P.A. 1996. 7-nitroindazole: an inhibitor of nitric oxide synthase. *Methods Enzymol.* **268**:393–398.
32. Reynaert, N.L., et al. 2004. Nitric oxide represses inhibitory kappaB kinase through S-nitrosylation. *Proc. Natl. Acad. Sci. U. S. A.* **101**:8945–8950.
33. Hu, M.C., et al. 2004. IkappaB kinase promotes tumorigenesis through inhibition of forkhead FOXO3a. *Cell.* **117**:225–237.
34. Segalat, L., Grisoni, K., Archer, J., Vargas, C., Bertrand, A., and Anderson, J.E. 2005. CAPON expression in skeletal muscle is regulated by position, repair, NOS activity, and dystrophy. *Exp. Cell Res.* **302**:170–179.
35. Shiao, T., et al. 2004. Defects in neuromuscular junction structure in dystrophic muscle are corrected by expression of a NOS transgene in dystrophin-deficient muscles, but not in muscles lacking alpha- and beta1-syntrophins. *Hum. Mol. Genet.* **13**:1873–1884.
36. Kapur, S., Bedard, S., Marcotte, B., Cote, C.H., and Marette, A. 1997. Expression of nitric oxide synthase in skeletal muscle: a novel role for nitric oxide as a modulator of insulin action. *Diabetes.* **46**:1691–1700.
37. Stamler, J.S., and Meissner, G. 2001. Physiology of nitric oxide in skeletal muscle. *Physiol. Rev.* **81**:209–237.
38. Yoshida, M., et al. 1995. Dystrophin-associated protein A0 is a homologue of the Torpedo 87K protein. *FEBS Lett.* **367**:311–314.
39. Yusuf, I., Zhu, X., Kharas, M.G., Chen, J., and Fruman, D.A. 2004. Optimal B-cell proliferation requires phosphoinositide 3-kinase-dependent inactivation of FOXO transcription factors. *Blood.* **104**:784–787.
40. Huang, H., Regan, K.M., Lou, Z., Chen, J., and Tindall, D.J. 2006. CDK2-dependent phosphorylation of FOXO1 as an apoptotic response to DNA damage. *Science.* **314**:294–297.
41. Kandarian, S.C., and Jackman, R.W. 2006. Intracellular signaling during skeletal muscle atrophy. *Muscle Nerve.* **33**:155–165.
42. Mochizuki, Y., et al. 2005. Participation of bone marrow-derived cells in fibrotic changes in denervated skeletal muscle. *Am. J. Pathol.* **166**:1721–1732.

Autologous Transplantation of SM/C-2.6$^+$ Satellite Cells Transduced with Micro-dystrophin *CS1* cDNA by Lentiviral Vector into *mdx* Mice

Madoka Ikemoto[1], So-ichiro Fukada[1], Akiyoshi Uezumi[1], Satoru Masuda[1], Hiroyuki Miyoshi[2], Hiroshi Yamamoto[3], Michiko R Wada[1], Nami Masubuchi[1,4], Yuko Miyagoe-Suzuki[1] and Shin'ichi Takeda[1]

[1]*Department of Molecular Therapy, National Institute of Neuroscience, National Center of Neurology and Psychiatry, Kodaira, Tokyo, Japan;* [2]*BioResource Center, RIKEN Tsukuba Institute, Tsukuba, Ibaraki, Japan;* [3]*Department of Immunology, Graduate School of Pharmaceutical Sciences, Osaka University, Suita, Osaka, Japan;* [4]*Laboratory of Molecular Embryology, Department of Bioscience, Kitasato University School of Science, Sagamihara, Kanagawa, Japan*

Duchenne muscular dystrophy (DMD) is a lethal muscle disorder caused by mutations in the dystrophin gene. Transplantation of autologous myogenic cells genetically corrected *ex vivo* is a possible treatment for this disorder. In order to test the regenerative efficiency of freshly isolated satellite cells, we purified quiescent satellite cells from limb muscles of 8–12-week-old green fluorescent protein-transgenic (GFP-Tg) mice using SM/C-2.6 (a recently developed monoclonal antibody) and flow cytometry. Freshly isolated satellite cells were shown to participate in muscle regeneration more efficiently than satellite cell-derived myoblasts passaged *in vitro* do, when transplanted into tibialis anterior (TA) muscles of 8–12-week-old cardiotoxin-injected C57BL/6 mice and 5-week-old dystrophin-deficient *mdx* mice, and analyzed at 4 weeks after injection. Importantly, expansion of freshly isolated satellite cells *in vitro* without passaging had no detrimental effects on their regenerative capacity. Therefore we directly isolated satellite cells from 5-week-old *mdx* mice using SM/C-2.6 antibody and cultured them with lentiviral vectors expressing micro-dystrophin *CS1*. The transduced cells were injected into TA muscles of 5-week-old *mdx* mice. At 4 weeks after transplantation, the grafted cells efficiently contributed to regeneration of *mdx* dystrophic muscles and expressed micro-dystrophin at the sarcolemma. These results suggest that there is potential for lentiviral vector-mediated *ex vivo* gene therapy for DMD.

Received 22 February 2007; accepted 28 July 2007; published online 28 August 2007. doi:10.1038/sj.mt.6300295

INTRODUCTION

Duchenne muscular dystrophy (DMD) is an X-linked, lethal disorder of skeletal muscle caused by mutations in the dystrophin gene.[1] Dystrophin is a 427 kd large sub-sarcolemmal protein that forms the dystrophin/glycoprotein complex at the sarcolemma with α- and β-dystroglycans, α-, β-, γ-, and δ-sarcoglycans, and other molecules, and links the cytoskeleton with the basal lamina.[2,3] The lack of dystrophin in the sarcolemma causes instability of the muscle membrane, leading to muscle degeneration and myofiber loss. Although there is no effective treatment for the disease at present, cell therapy could be a promising approach. Satellite cells are quiescent mononucleated cells located external to the muscle membrane but internal to the basal lamina in adult skeletal muscle.[4] On muscle damage, they activate, proliferate, and then exit the cell cycle either to differentiate into mature myofibers or to renew the quiescent satellite cell pool. Because satellite cells have robust regenerative capacity,[5,6] they are expected to be a feasible source for cell therapy in DMD. Indeed, transplantation of myoblasts successfully restored dystrophin expression in dystrophin-deficient muscle under immunosuppression.[7,8] Nevertheless, in the early 90s, transplantation of satellite cell-derived myoblasts failed to improve muscle force in DMD patients.[9–11] The failure has been ascribed to poor survival[12–14] and limited distribution of the transplanted cells after injection.[15] The latter problem could possibly be partly overcome by using high-density injections of myoblasts.[16,17] On the other hand, the mechanisms by which grafted myoblasts are rapidly lost after injection have not been fully addressed.[12–14]

Many studies have employed crude cell preparations containing both satellite cells and non-myogenic cells[18,19] or satellite cell-derived myoblasts extensively amplified *in vitro*.[15,20–22] In a recent study, Montarras *et al.* directly isolated (Pax3)green fluorescent protein (GFP)-expressing satellite cells from the diaphragm of adult *Pax3*$^{GFP/+}$ mice by flow cytometry.[23] These cells constituted a homogeneous population and the majority were quiescent. When grafted into irradiated muscles of immunodeficient *nu/nu* dystrophin-deficient *mdx* mice, the freshly isolated satellite cells efficiently contributed to both fiber repair and the muscle satellite cell compartment,[23] thereby suggesting that fresh satellite cells are a potential source for cell therapy in DMD.

For transplanting autologous cells, which are expected to evade the host immune response to grafted cells, the lentiviral vector is a potential tool for introducing the therapeutic gene

Correspondence: Shin'ichi Takeda, Department of Molecular Therapy, National Institute of Neuroscience, National Center of Neurology and Psychiatry, 4-1-1 Ogawa-higashi, Kodaira, Tokyo 187-8502, Japan. E-mail: takeda@ncnp.go.jp

because it integrates into the host genome in a variety of dividing and non-dividing cells. Because the dystrophin complementary DNA is too large to be incorporated into a lentiviral vector, a truncated but fully functional version of the dystrophin complementary DNA[24–27] has to be used instead of the full-length one. When compared with conventional transfection of myogenic cells with large dystrophin-coding plasmids[28] or nucleofection in combination with ϕC31 integrase,[29] transfection by lentiviral vectors led to much more efficient expression of mini- or micro-dystrophin in *mdx* mice,[30] in non-human primate cells, and in human myogenic cells.[31] Lentiviral vectors were also used for introducing the therapeutic genes into other types of stem cells. Bachrach *et al.* reported expression of human micro-dystrophin in mdx^{5cv} muscles after systemic delivery of autologous side population cells modified with lentiviral vectors expressing micro-dystrophin.[32] Sampaolesi *et al.* reported intra-arterial delivery of autologous mesoangioblasts corrected by lentiviral vectors expressing α-sarcoglycan (α-SG), resulting in many α-SG-positive fibers, and morphological and functional recovery in downstream muscles of α-SG-null dystrophic mice.[33] A more recent study reported the autologous transplantation into skeletal muscle, of monkey muscle precursor cells transduced with micro-dystrophin by lentiviral vectors.[31] However, whether *ex vivo* gene therapy using lentiviral vectors expressing micro-dystrophin is indeed beneficial in large animal models such as dystrophic dogs, is still subject to controversy.[34]

Previously, Fukada *et al.* established a method of direct purification of quiescent satellite cells from adult mouse skeletal muscles, using fluorescence activated cell sorting (FACS) and a novel monoclonal antibody named SM/C-2.6.[35] The method is simple, and is expected to be applicable to the isolation of satellite cells from dystrophic (autologous) muscles for cell therapy.

In this study, we first directly isolated satellite cells from *mdx* mice using the SM/C-2.6 antibody and FACS. We showed that *mdx*-SM/C-2.6$^+$ cells transduced with lentiviral vectors expressing micro-dystrophin efficiently contributed to regeneration of *mdx* muscles and expressed micro-dystrophin at the sarcolemma when grafted. Our results indicate that the autologous satellite cell isolated by the SM/C-2.6 antibody and genetically corrected by a lentiviral vector is a feasible tool for cell therapy of DMD or of localized forms of muscular dystrophy.

RESULTS

Passaged SM/C-2.6$^+$ satellite cells show reduced regenerative capacity

We isolated satellite cells from the limb muscles of 8–12-week-old C57BL/6 mice using FACS and a novel monoclonal antibody, SM/C-2.6.[35] A previous study has shown that satellite cells are highly enriched in the SM/C-2.6$^+$ fraction.[35] Immediately after isolation by FACS, SM/C-2.6$^+$ cells expressed Pax7, but not MyoD, myogenin, or Ki67 (**Table 1**). After 4 days of culture, more than 95% of the cells expressed MyoD and Ki67 (data not shown). Pax7 marks quiescent, activated satellite cells and their progeny, myoblasts,[36] whereas MyoD marks activated satellite cells and myoblasts.[37,38] Ki67 is a marker of proliferating cells. It follows, therefore, that SM/C-2.6$^+$ cells are highly purified satellite cells in the G_0 phase immediately after isolation from muscle tissues.

Table 1 Expression of myogenic and proliferative markers of freshly isolated SM/C-2.6$^+$ cells from limb muscles of C57BL/6 or *mdx* mice

Marker	B6-SM/C-2.6$^+$ cells (%)	*mdx*-SM/C-2.6$^+$ cells (%)
Pax7	95 ± 1.4	94 ± 2.1
MyoD	0 ± 0	19 ± 2.8
Myogenin	0 ± 0	7 ± 1.3
Ki67	0.6 ± 1.0	34 ± 1.8

The expression level of each marker is shown as the percentage of positive cells in total cells stained with 4′,6-diamidino-2-phenylindole in three randomly selected fields. Data are represented as mean values ± SD.

To investigate the regenerative efficiency of SM/C-2.6$^+$ satellite cells when grafted into mouse skeletal muscles, three kinds of cells were prepared from limb muscles of 8–12-week-old GFP-Tg mice: (i) quiescent SM/C-2.6$^+$ cells freshly isolated by FACS (**Figure 1a**), (ii) expanded SM/C-2.6$^+$ cells *in vitro* with or without passaging (**Figure 1a**), and (iii) cultured primary myoblasts isolated by a conventional pre-plating method.[39] These cells were injected at 2×10^4 cells per muscle into the tibialis anterior (TA) muscle of 8–12-week-old C57BL/6 and 5-week-old dystrophin-deficient *mdx* mice. Twenty four hours before cell transplantation the recipient C57BL/6 muscles were injected with cardiotoxin (CTX) so as to induce regeneration. Four weeks after the injection, we investigated the contribution of each cell population to muscle regeneration by immunodetection of GFP-positive fibers. Freshly isolated SM/C-2.6$^+$ cells (**Figure 1b**) produced many more GFP-positive fibers than those produced by the same number of cultured SM/C-2.6$^+$ cells passaged once *in vitro* (**Figure 1c**, passage 1). We next examined the effects of expansion, without passaging and with repeated passaging, on the regenerative capacity of the cells. The number of GFP-positive myofibers derived from GFP-Tg SM/C-2.6$^+$ cells dropped considerably after first passage *in vitro* and then gradually decreased with subsequent passages in both CTX-injected C57BL/6 mice (**Figure 1d**) and in *mdx* mice (**Figure 1e**). Primary myoblasts prepared by the pre-plating method[39] also showed low regenerative capacity (**Figure 1d**). Surprisingly, the regenerative efficiency of cells expanded *in vitro* without passaging was comparable to that of freshly isolated cells (**Figure 1d** and **e**). These results suggested to us that it is possible to genetically correct dystrophin-deficient satellite cells *ex vivo* before transplantation without causing a reduction in their regenerative capacity.

In order to know why fresh or "expansion" cells gave rise to more myofibers when compared with cells passaged *in vitro*, we compared the colony formation ability of fresh satellite cells with that of passaged myoblasts (passage 1). The results showed that fresh satellite cells formed larger colonies than passage 1 cells, when plated at a density of 1 cell/well on 96-well plates, although the rate of colony formation was not significantly different between these two cells (fresh, 26% versus passage 1, 23%) (**Supplementary Figure S1**). In contrast, there was no difference in fusion index between fresh satellite cells and passaged myoblasts (data not shown). Collectively, a reduction in the proliferative ability of passaged myoblasts *in vitro* might partly explain their lower regenerative capacity *in vivo*.

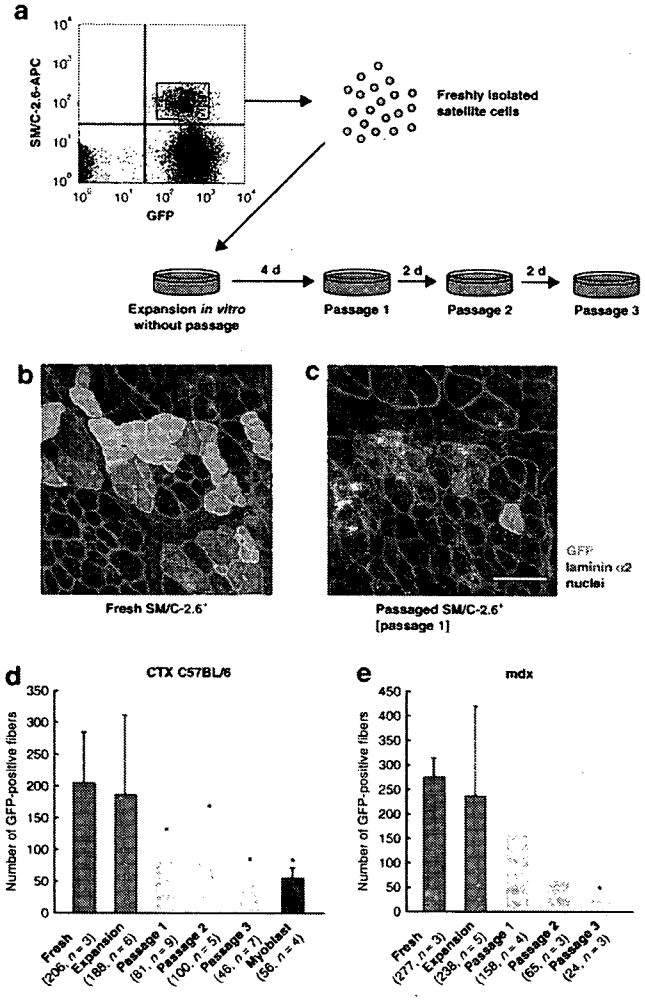

Figure 1 The regenerative capacity of SM/C-2.6$^+$ satellite cells isolated from adult mouse skeletal muscles by fluorescence activated cell sorting (FACS). (**a**) Flow cytometry of mononucleated cells derived from limb muscles of green fluorescent protein-transgenic (GFP-Tg) mice after staining with SM/C-2.6 antibody and culture conditions of sorted cells. SM/C-2.6$^+$ GFP$^+$ cells (red square) were sorted as the satellite cell fraction. These cells were cultured in proliferation medium for 4 days (expansion *in vitro* without passage) and then passaged up to three times at 2-day intervals. (**b**) Freshly isolated and (**c**) passaged SM/C-2.6$^+$ cells (passage 1) from GFP-Tg mice were injected into C57BL/6 tibialis anterior (TA) muscles. The muscles were treated with cardiotoxin (CTX) 24 hours before cell transplantation and then injected with 2 × 10^4 cells per TA muscle. Four weeks after the injection, cross-sections were stained with anti-GFP (green) and laminin α2 (red) antibodies. Nuclei were stained with TOTO3 (blue). Bar: 80 μm. (**d**, **e**) Comparison of muscle regenerative efficiencies of three kinds of cells prepared from GFP-Tg mice: (i) quiescent SM/C-2.6$^+$ cells freshly isolated by FACS (red bars), (ii) expanded SM/C-2.6$^+$ cells *in vitro* without passaging (orange bars) or passaged SM/C-2.6$^+$ cells (yellow bars with passage numbers), and (iii) primary myoblasts isolated by the preplating method (blue bar in **d**). The same numbers of cells (2 × 10^4 cells) were grafted into TA muscles of CTX-treated C57BL/6 (d) and *mdx* mice (**e**). The number of GFP-positive fibers per cross-section was counted after staining with anti-GFP antibody. Error bars represent SD. $^*P < 0.05$ compared with freshly isolated SM/C-2.6$^+$ cells.

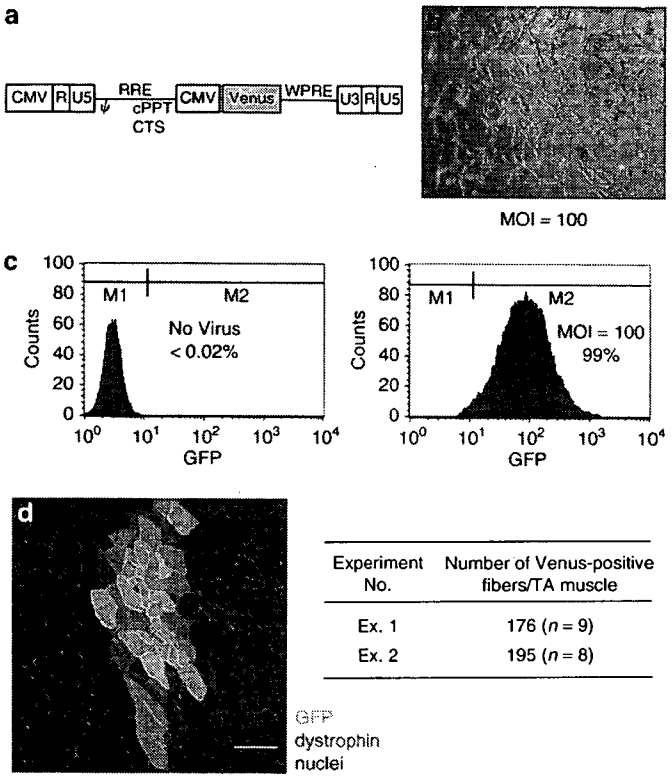

Experiment No.	Number of Venus-positive fibers/TA muscle
Ex. 1	176 (n = 9)
Ex. 2	195 (n = 8)

Figure 2 Lentiviral vector-mediated gene transfer into SM/C-2.6$^+$ satellite cells and transplantation of transduced cells into *mdx* mouse muscles. (**a**) Structure of the lentiviral vector expressing Venus under the control of a cytomegalovirus (CMV) promoter. (**b**) Fluorescence of Venus-expressing satellite cell-derived myoblasts. Freshly isolated SM/C-2.6$^+$ cells from C57BL/10 limb muscles were transduced with lentiviral vectors expressing Venus at a multiplicity of infection (MOI) of 100 for 16 hours, and cultured in proliferation medium for 3 days. (**c**) Flow cytometric analysis of non-transduced (left panel) and transduced (right panel) SM/C-2.6$^+$ cells 3 days after the transduction. M2 denotes the area of Venus-expressing cells. At a MOI of 100, 99% of the cells expressed Venus. (**d**) Venus- and dystrophin-positive fibers formed by SM/C-2.6$^+$ cells transduced with lentiviral vectors *in vitro*. Transduced cells (2 × 10^4) were injected into tibialis anterior (TA) muscles of *mdx* mice. Four weeks after the injection, cross-sections were stained with anti-GFP (green) and dystrophin (red) antibodies. Nuclei were stained with TOTO3 (blue). The number of Venus-positive fibers per cross-section was counted. Bar: 80 μm. cPPT, central polypurine tract; CTS, central termination sequence; GFP, green fluorescent protein; RRE, rev responsive element; WPRE, woodchuck hepatitis virus post-transcriptional regulatory element.

SM/C-2.6$^+$ satellite cells transduced with lentiviral vectors efficiently contribute to muscle regeneration

Successful gene and cell therapy for DMD requires sustained expression of the therapeutic gene in striated muscle. The lentiviral vector can carry a relatively large transgene and integrate it into the genome of non-dividing cells such as quiescent satellite cells. We therefore attempted lentiviral vector–mediated gene transfer into satellite cells. For this purpose, we used a human immunodeficiency virus-1–based lentiviral vector pseudotyped with vesicular stomatitis virus-G glycoprotein.[40] To start with, we used a vector that expresses Venus, a variant of yellow fluorescent protein[41] under the control of a cytomegalovirus (CMV) promoter (**Figure 2a**). Freshly isolated satellite cells from limb muscles of 8–12-week-old C57BL/10 mice, which are syngenic to *mdx*, were transduced with the lentiviral vectors at a multiplicity of infection (MOI) of 100 for 16 hours. After removal of free viral vectors and *in vitro* expansion of the cells for 3 days, numerous Venus-positive cells were detected (**Figure 2b**). Flow

cytometric analyses revealed that 99% of the SM/C-2.6$^+$ satellite cell-derived myoblasts expressed Venus when transduced at a MOI of 100 (**Figure 2c**, right panel). These transduced cells were injected into TA muscles of 5-week-old *mdx* mice at 2×10^4 per muscle. Four weeks after the injection, the muscle regeneration capacity of cells transduced with lentiviral vectors was investigated by immunodetection of Venus- or dystrophin-positive fibers. As in the case of the non-transduced cells (**Figure 1d and e**), grafting of transduced cells too led to many Venus- and dystrophin-positive fibers (**Figure 2d**). This serves to show that SM/C-2.6$^+$ satellite cell-derived myoblasts transduced with lentiviral vectors contribute efficiently to muscle regeneration.

Direct isolation of SM/C-2.6$^+$ satellite cells from dystrophic muscles of *mdx* mice

In order to test whether autologous myogenic precursor cells genetically corrected to express a dystrophin gene represent a possible tool in DMD therapy, we next attempted to directly isolate SM/C-2.6$^+$ cells from limb muscles of 5-week-old *mdx* mice. Numerous inflammatory and fibroblastic cells reflecting the active cycles of the degeneration–regeneration process are found in dystrophic muscles. SM/C-2.6 antibody reacts with activated fibroblastic cells (Fukada *et al.*, unpublished data). Because satellite cells are negative for both Sca-1 and CD31,[35] we stained *mdx* muscle-derived mononuclear cells with a cocktail of CD45, CD31, Sca-1, and SM/C-2.6 antibodies and collected SM/C-2.6$^+$ CD45$^-$ CD31$^-$ Sca-1$^-$ cells as the satellite cell fraction (**Figure 3a**). When these cells were cultured in proliferation medium for 4 days, more than 95% of them expressed MyoD (**Figure 3b**). These results indicate that, using the SM/C-2.6 antibody, a pure population of satellite cells can be isolated, not only from wild-type muscle but also from dystrophic muscle of *mdx* mice. Immediately after isolation, the majority of satellite cells from C57BL/6 mice were negative for MyoD, myogenin, and Ki67. On the other hand, 19% of *mdx*-satellite cells were positive for MyoD and 34% of the cells were positive for Ki67 (**Table 1**). There was no difference between *mdx*- and B6-SM/C-2.6$^+$ cells with respect to expression of Pax7 (**Table 1**). This proves that a considerable fraction of satellite cells are in an activated, proliferative state in skeletal muscles of *mdx* mice.

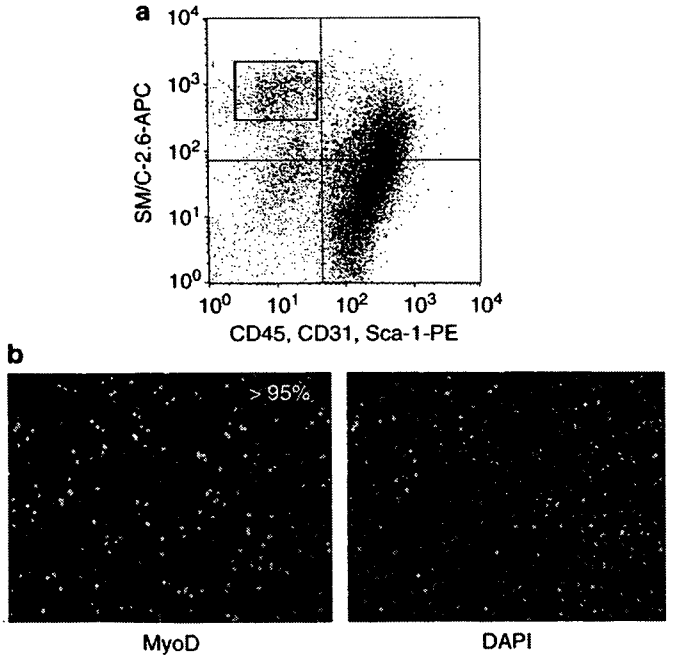

Figure 3 Direct isolation of SM/C-2.6$^+$ satellite cells from dystrophic muscles of *mdx* mice. (**a**) Flow cytometry of mononucleated cells derived from *mdx* mice, and stained with a cocktail of CD45, CD31, Sca-1, and SM/C-2.6 antibodies. SM/C-2.6$^+$ CD45$^-$ CD31$^-$ Sca-1$^-$ cells (red square) were sorted as the satellite cell fraction. (**b**) Sorted *mdx*-satellite cells were cultured in proliferation medium for 4 days and stained with anti-MyoD antibody (green) and 4′,6-diamidino-2-phenylindole (DAPI) (nuclei, blue). More than 95% of them expressed MyoD.

Successful micro-dystrophin gene transfer into *mdx*-SM/C-2.6$^+$ satellite cells

The full-length dystrophin complementary DNA, at 14 kilobase (kb), is too large to be incorporated into a lentiviral vector. In previous studies, we constructed a rod-truncated micro-dystrophin *CS1* and demonstrated that it effectively rescued

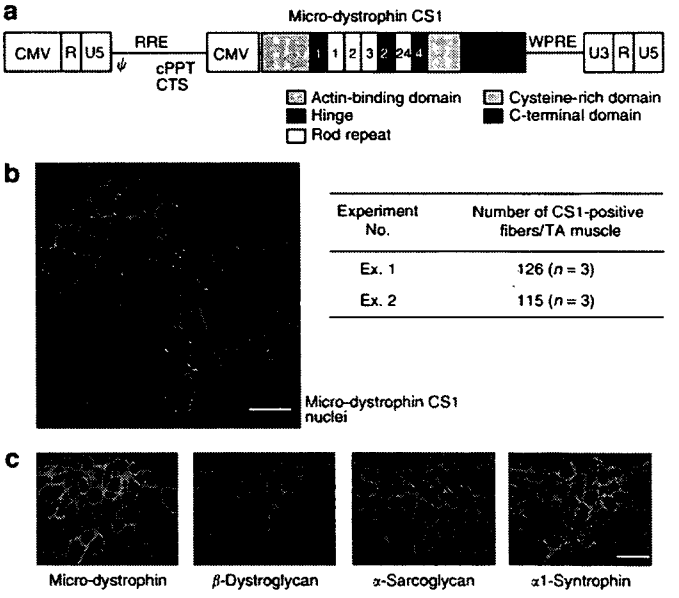

Figure 4 Lentiviral vector-mediated micro-dystrophin *CS1* gene transfer into *mdx*-SM/C-2.6$^+$ cells and transplantation of transduced cells into *mdx* muscles. (**a**) Structure of the lentiviral vector expressing micro-dystrophin *CS1*. *CS1* complementary DNA was inserted downstream of the cytomegalovirus (CMV) promoter. *CS1* has the N-terminal domain, a shortened version of the central rod domain with four rod repeats and three hinges, the cysteine-rich domain, and the C-terminal domain. The numbers of rod repeats and hinges are also shown. (**b**) Freshly isolated SM/C-2.6$^+$ cells from *mdx* dystrophic muscles were transduced with lentiviral vectors expressing micro-dystrophin *CS1* at a multiplicity of infection of 200 for 16 hours and cultured in proliferation medium for 2 days. Transduced cells (2×10^4) were injected into *mdx* tibialis anterior (TA) muscles. Four weeks after the injection, cross-sections were stained with anti-dystrophin antibody (red) and TOTO3 (nuclei, blue). The number of micro-dystrophin *CS1*-positive fibers per cross-section was counted. Bar: 80 μm. (**c**) Restoration of dystrophin-associated proteins at the sarcolemma of micro-dystrophin-positive fibers. Serial cross-sections were stained with anti-dystrophin, β-dystroglycan, α-sarcoglycan, and α1-syntrophin antibodies (red), and TOTO3 (nuclei, blue). Bar: 80 μm. cPPT, central polypurine tract; CTS, central termination sequence; RRE, rev responsive element; WPRE, woodchuck hepatitis virus post-transcriptional regulatory element.